THE KINETICS OF NON-CATALYZED SUPERCRITICAL WATER REFORMING OF ETHANOL

A Dissertation presented to the
Faculty of the Graduate School
University of Missouri—Columbia

In Partial Fulfillment
of the Requirements for the Degree

Doctor of Philosophy

---

by
JONATHAN E. WENZEL

Dr. Sunggyu Lee, Dissertation Advisor

MAY 2008

© Copyright by Jonathan E. Wenzel 2008
All Rights Reserved

The undersigned, appointed by the Dean of the Graduate School, have examined the dissertation entitled

THE KINETICS OF NON-CATALYZED SUPERCRITICALWATER REFORMING OF ETHANOL

Presented by Jonathan E. Wenzel

A candidate for the degree of Doctor of Philosophy

And hereby certify that in their opinion it is worthy of acceptance.

_____
Professor Sunggyu Lee

_____
Professor David Retzloff

_____
Professor Stephen Lombardo

_____
Professor Sudarshan Loyalka

_____
Professor John Adams

For my parents, Kurt and Donna, for the constant love that they show, the support that they give, and the faith that they have in me. I am most fortunate to have the parents I have.

For my family and friends who are always there for me.

ACKNOWLEDGEMENTS

I would like to thank Dr. Sunggyu Lee my dissertation advisor for allowing me to work in his group. It has been an honor and a privilege. I would especially like to thank him for the world class education that he provided me in preparation for life both inside and out of the laboratory. I would also like to thank my co-workers, Dr. H. Bryan Lanterman, Mr. Jason Picou, and Ms. Alexandria Niemoeller. Dr. Lanterman was an invaluable sounding board for my ideas. Jason provided invaluable assistance in the up-keep and operations of the supercritical water reformer and the gas chromatograph calibrations that made my work possible. Lexie provided help with reformer operations and weighing all of the liquid samples that I collected.

TABLE OF CONTENTS

LIST OF FIGURES

LIST OF TABLES

THE KINETICS OF NON-CATALYZED SUPERCRITICAL WATER REFORMING OF ETHANOL

Jonathan E. Wenzel

Dr. Sunggyu Lee, Dissertation Supervisor

ABSTRACT

Agriculturally produced ethanol, a renewable resource, may be reformed non-catalytically into hydrogen by a novel process utilizing supercritical water, which acts synergistically both as a solvent and as a reactant. By utilizing supercritical water as a reaction medium, many pitfalls of catalytic reformation may be avoided, including catalyst poisoning due to feedstock impurities, catalyst fouling by carbon deposition, and catalyst deactivation. Supercritical water is water above its critical point, 374°C and 22.1 MPa, and exhibits both liquid and gas-like properties and acts a non-polar solvent. Since supercritical water is denser than steam, supercritical water reactors have the potential of being smaller than their catalytic counterparts.

The kinetics of supercritical water reformation of ethanol were experimentally studied using a 1 liter Inconel® 625 Grade 1 alloy tubular reactor. For the experimental study, the temperature was varied between 901 K and 983 K, the water feed rate was varied between 6.4 g/min and 19.7 g/min, the ethanol feed rate was varied between 0.17 g/min and 2.2 g/min, and the pressure was fixed at 24.2 MPa. All ethanol fed was converted into gaseous products: hydrogen, carbon dioxide, methane, ethane, and carbon monoxide, in order of mole fraction from highest to lowest.

Hydrogen was produced by two competing reactions: the direct reformation of ethanol into hydrogen and carbon oxides and the pyrolytic decomposition of ethanol into hydrogen, methane, and carbon oxides. In addition, there is a third, undesirable, reaction

that remarkably occurs in a water-rich environment: the dehydration of ethanol to form ethene and the subsequent hydrogenation of ethene to form ethane. In addition, a low abundance of carbon monoxide in relation to carbon dioxide is indicative that the forward water-gas shift reaction is taking place. Arrhenius activation energies for the direct reformation reaction and the pyrolytic decomposition reaction were also regressed.

CHAPTER 1

INTRODUCTION

1.1 Research Objective

The objective of this work is to determine the reaction kinetic information of the reformation of ethanol in a non-catalyzed environment using supercritical water. For this work, seventeen experiments were devised and performed to determine the parameters for a kinetic model based on three stoichiometric equations: the direct reformation of ethanol, the water-gas shift reaction (WGS), and the decomposition of ethanol. In addition, the effects of the process conditions, such as temperature, residence time, and reactant concentrations, will be examined and analyzed.

1.2 Research Motivation

Ethanol, produced from the fermentation of grains and other biomass, is a safe, renewable, and potentially attractive domestically produced fuel source. Ethanol is currently blended with gasoline in small amounts as a replacement for MTBE to improve automotive emissions. In addition, E-85, an 85% ethanol/15% gasoline blend is currently available as a transportation fuel for flex-fuel vehicles. However, there are several issues that are confronting the petroleum industry when blending ethanol into gasoline or for use as a gasoline substitute.

A primary issue is ethanol's affinity for water, which poses problems from ethanol production to distribution to combustion. Binary mixtures of ethanol and water cannot be completely distilled due to the azeotrope of water and ethanol at 89.43 mole-%

water and 10.57 mole-% ethanol.[1] This necessitates more energy-intensive means of separation such as secondary distillation with pentane. Most carriers will not distribute ethanol-blended fuels in their pipelines due to water contamination issues and an increased risk for corrosion.[2] Due to water's high heat of vaporization and high heat capacity[3], water contaminated fuels lower the amount of energy that may be obtained during combustion. Finally, ethanol's energy density is two-thirds that of gasoline, resulting in a lower fuel economy when measured by miles per gallon.

However, ethanol, other alcohols, and hydrocarbons can be reformed into hydrogen, which could make ethanol attractive in a hydrogen-based economy. Ethanol's affinity for water is a benefit, instead of a drawback, in steam-reforming, and the resulting hydrogen is readily separated from the reactants. In order to better understand ethanol reforming, it is necessary to have a kinetic model of the chemical reactions that occur during reformation. A kinetic understanding is essential for reactor sizing, reactor design, process optimization, and economic optimization.

1.3 Motivation for Supercritical Water

Supercritical water is water above its critical point, T_c=374°C and P_c=22.064 MPa.[4] Supercritical water has been successfully demonstrated as a reaction medium for hydrocarbon reformation of methanol[5] and higher carbon-number fuels such as diesel and military logistic fuel.[6] For fuel reformation to hydrogen, supercritical water acts synergistically both as a solvent and as a reactant. Supercritical water exhibits both liquid and gas-like properties, and as a result permits the variation of transport and thermodynamic properties (i.e., diffusivity, surface tension, thermal conductivity,

viscosity, etc.) by changing the temperature and/or density of the supercritical medium. It is also important to note that the dielectric constant of water decreases as the temperature and pressure approach the critical point, resulting in water being a more non-polar than polar solvent. In addition, supercritical water reformation avoids many of the pitfalls of catalytic steam reformation including: catalyst poisoning from impurities in the feed-stock, such as sulfur; catalyst deactivation due to coking and fouling; sintering; need for catalyst regeneration; and etc.

CHAPTER 2

BACKGROUND

2.1 Catalytic Steam Reforming of Ethanol

Several different catalysts have been tried and tested for facilitating steam reforming of ethanol. Oxide catalysts include alumnia, vanadia, and zinc oxide. Oxide-supported metal catalysts include using metals such as cobalt, nickel, copper, or rhodium supported by alumina, vanadia, zinc oxide, etc.[7] Several different kinetic pathways and chemical mechanisms have been proposed.

2.2 Proposed Chemical Reactions for Steam Reforming of Ethanol.

Depending upon the temperature and the presence of a catalyst, several reaction pathways for the reforming of ethanol have been proposed to take place, and several products or intermediates have been proposed to be formed. These products include hydrogen, carbon monoxide, carbon dioxide, methane, ethane, ethene, acetaldehyde, acetone, acetic acid, and coke.[7] Reaction pathways include dehydration of ethanol to form acetaldehyde and ethene, decarbonylation of acetaldehyde to form methane and carbon monoxide, and the decomposition of ethanol to form methane, carbon dioxide, and hydrogen. Overall, the stoichiometric equation for steam reforming of ethanol may be represented as

$$C_2H_5OH + 3\ H_2O \rightarrow 2\ CO_2 + 6H_2 \qquad (2.1)$$

alternatively, the reforming reaction may be represented as

$$C_2H_5OH + H_2O \rightarrow 2\ CO + 4\ H_2 \qquad (2.2)$$

which could be considered (2.1) combined with the forward water-gas shift reaction

$$CO + H_2O \rightarrow CO_2 + H_2 \qquad (2.3)$$

2.2.1 Reactions involving the Dehydration of Ethanol

The dehydration reaction of ethanol is relatively active in nickel-alumina catalyzed reactions at low temperatures (less than 100°C) and becomes more active with increasing temperature.[8] This possible pathway competes with ethanol reformation. It may result in fouling and coking of the catalyst and may consume the desired product, hydrogen, by hydrogenation. The dehydration reaction is stoichiometrically represented by

$$C_2H_5OH \rightarrow C_2H_4 + H_2O \qquad (2.4)$$

Ethene may then be polymerized to form coke:

$$C_2H_4 \rightarrow \text{coke} + H_2 \qquad (2.5)$$

Ethene may also be hydrogenated to form ethane:

$$C_2H_4 + H_2 \rightarrow C_2H_6 \qquad (2.6)$$

2.2.2 Reactions involving the Dehydrogenation of Ethanol

A possible chemical pathway for the reformation of ethanol, both with or without a catalyst, is the dehydrogenation of ethanol to form acetaldehyde:

$$C_2H_5OH \rightarrow C_2H_4O + H_2 \qquad (2.7)$$

This reaction has been observed at temperatures below 300°C in a copper-plated Raney nickel catalyzed reactor and over a wide variety of other catalysts.[9]

Acetaldehyde can also undergo decarbonylation to form methane and carbon monoxide:

$$C_2H_4O \rightarrow CH_4 + CO \qquad (2.8)$$

This decomposition occurs very quickly, with acetaldehyde concentrations becoming negligible, in rhodium-cerium oxide catalyzed systems at temperatures above 650°C.[10]

It is also possible for acetaldehyde to undergo further steam reforming reaction:

$$C_2H_4O + H_2O \rightarrow 2\ CO + 3\ H_2 \qquad (2.9)$$

which occurs in many different catalyzed systems, including rhodium-alumia.[11]

2.2.3 Carbon Monoxide

Carbon monoxide during steam reformation may participate in several different reactions depending on the temperature and the presence of a catalyst. At temperatures below 500°C in nickel-based catalyst systems, carbon monoxide and carbon dioxide can undergo methanation reactions[8]:

$$CO + 3\ H_2 \rightarrow CH_4 + H_2O \qquad (2.10)$$

$$CO_2 + 4\ H_2 \rightarrow CH_4 + 2\ H_2O \qquad (2.11)$$

In catalyzed environments, the forward water-gas shift reaction is also active[7, 11, 12]:

$$CO + H_2O \rightarrow CO_2 + H_2 \qquad (2.3)$$

Carbon monoxide and carbon dioxide may also contribute to coking via the Boudouard reaction[7, 8, 10]:

$$2\ CO \rightarrow CO_2 + C \qquad (2.12)$$

$$CO_2 \rightarrow C + O_2 \qquad (2.13)$$

2.2.4 Chemical Reactions involving Methane

Methane is typically steam-reformed over nickel-based catalysts to form carbon monoxide and hydrogen:

$$CH_4 + H_2O \rightarrow CO + 3\ H_2 \qquad (2.14)$$

which is typically reformed between 700-800°C.[13] In addition methane may be a source of fouling[7, 10, 13]:

$$CH_4 \rightarrow \text{higher order polyaromatic hydrocarbons} \qquad (2.15)$$

2.2.5 Non-catalytic Reformation

Ethanol may also be reformed non-catalytically using supercritical water.[5] Arita et al. performed several batch experiments at 500°C in a sealed quartz tube reactor at various reaction times, the minimum being 10 minutes and maximum 60 minutes.[14] Ethanol was completely reacted to produce hydrogen, acetaldehyde, methane, carbon dioxide, carbon monoxide, ethylene, and ethane. They proposed the following two parallel pathways for the decomposition of ethanol:

Pathway 1:
$$C_2H_5OH \rightarrow CH_3CHO + H_2 \qquad (2.8)$$
$$CH_3CHO \rightarrow CH_4 + CO \qquad (2.9)$$
$$CO + H_2O \rightarrow CO_2 + H_2 \qquad (2.3)$$

Pathway 2:
$$C_2H_5OH \rightarrow C_2H_4 + H_2O \qquad (2.4)$$
$$C_2H_4 + H_2 \rightarrow C_2H_6 \qquad (2.6)$$

At 500°C after 60 minutes of reaction, hydrogen made up approximately 44 mol-% and acetaldehyde 28 mol- % of the decomposition products of ethanol. The initial rate constant for the decomposition of ethanol into acetaldehyde was reported to be 3.52×10^{-5} s^{-1} at a water density of 0.20 g cm^{-3} at 500°C.

2.2.6 Water Gas Shift Reaction in Supercritical Water

In commercial practices, the first stage for water-gas shift is also typically the highest-temperature stage, using an iron/chromium catalyst for temperatures between 320 and 360°C.[15] The water gas shift reaction is a reversible equilibrium-limited reaction over a wide temperature range. Using data from the JANAF tables[16], the equilibrium constants for the water-gas shift reaction are plotted as a function of temperature in Figure 2.1.

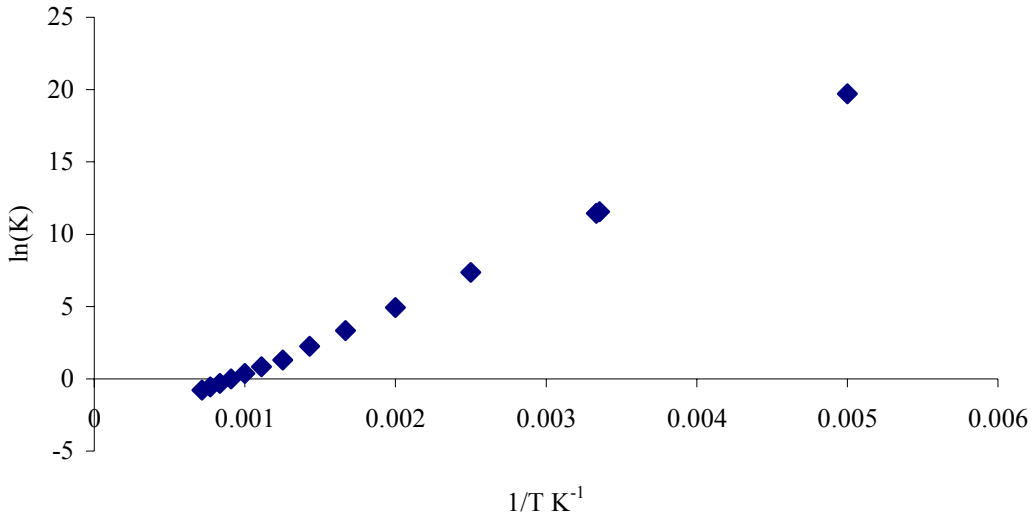

Figure 2.1: Equilibrium constant of the water gas shift reaction as a function of temperature.

The cross-over temperature between the forward and reverse shift reactions is 1074 K. As such, the forward water-gas shift reaction also occurs in supercritical water under appropriate imposed conditions. An experimental study using a 383-mL tubular Haynes® Alloy 230 reactor demonstrated that the forward water-gas shift reaction can reach 98.9% conversion in supercritical water at 1045 K and 22.4 MPa. The water feed rate was 16.1 g·min^{-1}, and the carbon monoxide feed rate was 0.5 SLPM.[17]

2.3 Supercritical Water and its Interaction with Intermediates

Ordinary water (non-deuterated) has a critical point of T_c=374°C and P_c=22.064 MPa, and water is in the supercritical fluid region at temperatures and pressures above this point.[4] The phase boundaries of water, generated from correlations printed in a circular from the International Association for the Properties of Water and Steam[18] is shown in Figure 2.2.

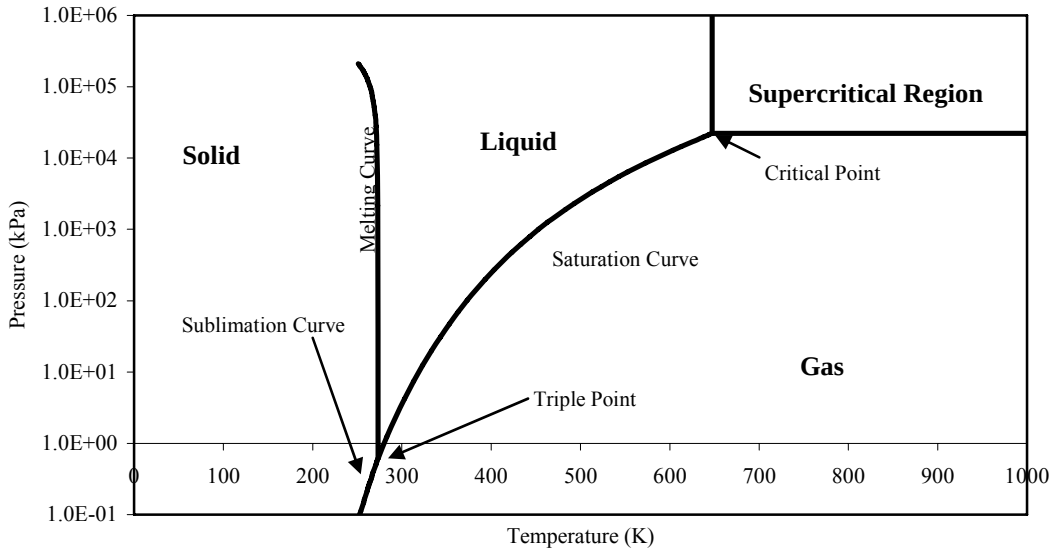

Figure 2.2: Phase diagram of water.

Above the critical point, water will exhibit both liquid and gas-like properties which are dependant upon temperature and pressure. Heat capacity, thermal conductivity, viscosity, and electrolytic conductivity can be varied by changes in the temperature and pressure of supercritical water. In addition, as the temperature and pressure of water increases up to the critical point of water, the dielectric constant decreases from 87.96 at ambient conditions to 6.19 at the critical point.[19] As a result, supercritical water may be classified as a non-polar solvent, which can readily dissolve other non-polar compounds such as hydrocarbons and form supercritical mixtures.

2.3.1 Molar Volume Estimation of Supercritical Water and Ethanol

In order to estimate the residence time for supercritical water reformation in a flow reactor, it is necessary to estimate the molar volume of supercritical water and any solute of choice. For the purposes of this work, the Peng-Robinson-Stryjek-Vera equation of state (PRSV-2) is used, which is expressed in the following form[20, 21]

$$P = \frac{R\,T}{v-b} - \frac{a(T)}{v(v+b)+b(v-b)} \tag{2.1}$$

where

$$a = 0.457235\,\alpha\frac{R^2T_c^2}{P_c} \tag{2.2}$$

$$b = 0.077796\,\frac{RT_c}{P_c} \tag{2.3}$$

and

$$\alpha = \left[1+\kappa_0\left(1-T_r^{0.5}\right)\right]^2 \tag{2.4}$$

$$\kappa_0 = 0.378893 + 1.4897153\,\omega - 0.17131848\,\omega^2 + 0.0196544\,\omega^3 \tag{2.5}$$

the attractive interaction parameter, a, for a mixture is expressed by

$$a = \sum_i^N \sum_j^N x_i x_j a_{ij} \tag{2.6}$$

where

$$a_{ij} = \left(1-k_{ij}\right)\sqrt{a_i a_j} \tag{2.7}$$

if $i \neq j$, then $a_{ij}=a_{ji}$, and if $i=j$, then the binary interaction parameter k_{ij} is zero. The covolume of the mixture, b, is expressed by

$$b = \sum_i^N x_i b_i \tag{2.8}$$

P is pressure, T is temperature, v is molar volume, R is the universal gas constant, κ_0 is a function of the accentric factor, and ω is the accentric factor. Subscripts c and r denote critical properties and reduced properties respectively.

For water-ethanol binary mixtures, the binary interaction parameter is -0.051866.[22] Critical properties for several species of interest to the current research are listed in Table 2.1.[4]

Table 2.1: Critical and physical properties of some species present in ethanol reforming.

Species	H_2O	CH_3CH_2OH	H_2	CO	CO_2	CH_4	C_2H_6
CAS #	7732-18-5	64-17-5	1333-74-0	630-08-0	124-38-9	74-82-8	74-84-0
MW	18.015	46.069	2.016	28.01	44.01	16.043	30.07
T_c/K	647.14	513.92	32.98	132.85	304.12	190.56	305.32
P_c/bar	220.64	61.48	12.93	34.94	73.74	45.99	48.72
$V_c/cm^3 \cdot mol^{-1}$	55.95	167	64.2	93.1	94.07	95.6	145.5
Z_c	0.229	0.24	0.303	0.292	0.274	0.286	0.279
ω	0.344	0.649	-0.217	0.045	0.225	0.011	0.099

2.3.2 Critical Locus of Water-Ethanol Mixtures

In order to ensure that the reactant mixture at the inlet of a supercritical reactor is in the supercritical region, it is necessary to have experimental vapor-liquid equilibrium data along the critical envelope or determine the critical locus of a mixture by an equation of state. Figure 2.3 is a plot of experimentally determined critical temperature data for binary mixtures of ethanol and water. Figure 2.4 is a plot of experimentally determined critical pressure data for binary mixtures of ethanol and water.[23] Ethanol and water exhibit Type I phase behavior with a continuous critical mixture curve from the heavier component, ethanol, to the lighter component, water.[24] Even though the critical properties of the ethanol-water mixture are more readily and accurately predictable, the fluid mixture along the reactor length is far from being similar to the original reactant

mixture due to influxes of reaction intermediates, products and byproducts. A detailed thermodynamic analysis of the critical and supercritical behavior of this multi-component fluid mixture along with the varying composition along the length of the reactor is not an immediate research objective of the current dissertation.

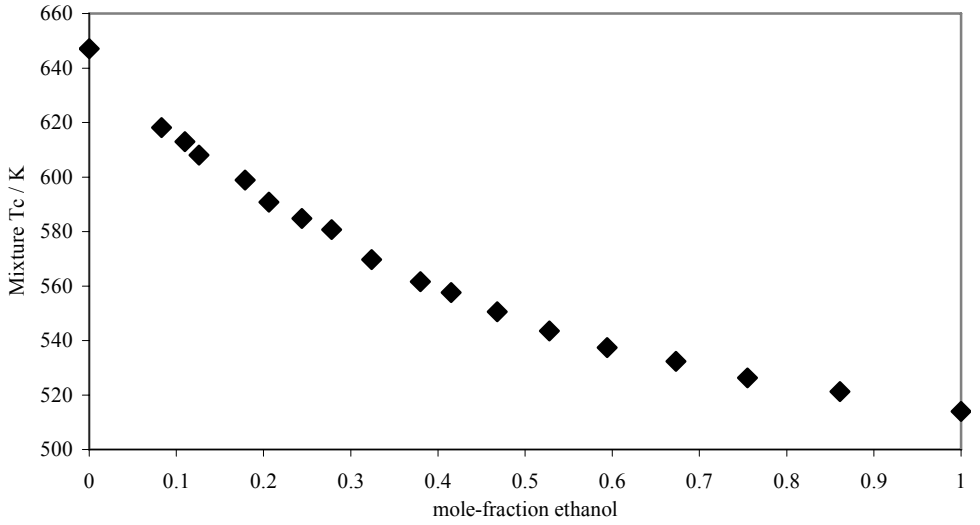

Figure 2.3: Experimentally determined critical temperature of mixtures of ethanol and water[23].

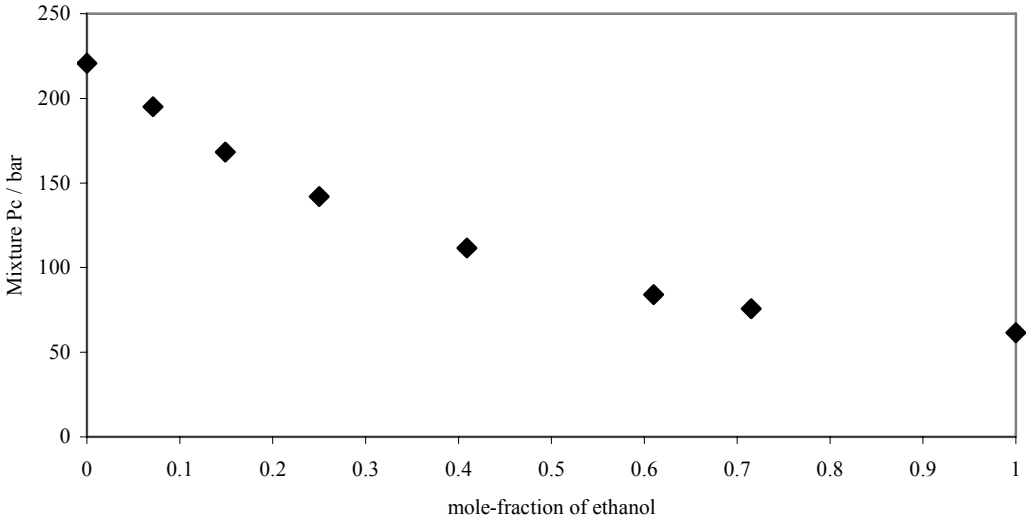

Figure 2.4: Experimentally determined critical pressure of mixtures of ethanol and water[23].

2.3.3 Critical Locus of Water-Product Mixtures

Fluid-phase behavior and mixture properties of water and reformation intermediates and products may have an influence on reactions and reaction rates. Though binary mixtures of water with alcohols and ketones typically have Type I phase diagrams, other mixtures of water with species of interest typically exhibit Type II and Type III phase behavior.[25]

Type II phase behavior is similar to Type I phase behavior with a continuous critical line. However, with Type II behavior, there is a liquid-liquid-vapor equilibrium region on the pressure/temperature projection ending at an upper critical end point where the liquid-liquid-vapor phase merges to form a single liquid phase.[24] An example of Type II phase behavior is the binary mixture of water and naphthalene, a polycyclic aromatic hydrocarbon and a potential product of coke formation, as shown in Figure 2.5.[26] Naphthalene's critical temperature is 748.4 K, and its critical pressure is 40.5 bar.[4]

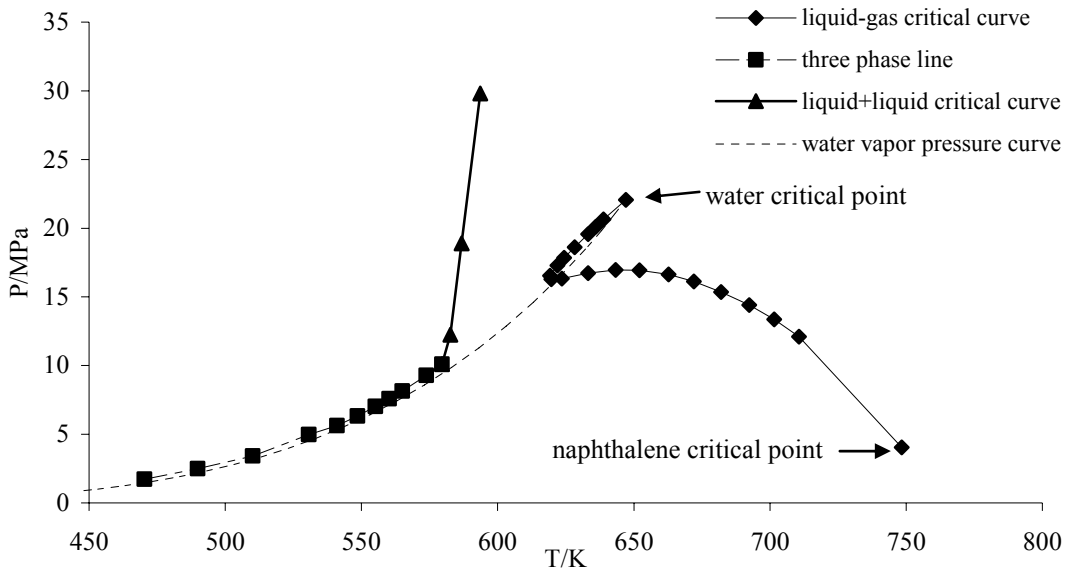

Figure 2.5: Pressure-temperature projection of mixtures of naphthalene and water[26].

Type III phase behavior is characterized by a discontinuous critical line and a liquid-liquid-vapor region close to the critical point of the more volatile component. Binary mixtures with dissimilar critical properties will typically exhibit Type III phase behavior.[24] An example of Type III phase behavior is the binary mixture of water and benzene, an aromatic hydrocarbon that is a potential coke precursor, as shown in Figure 2.6.[26]

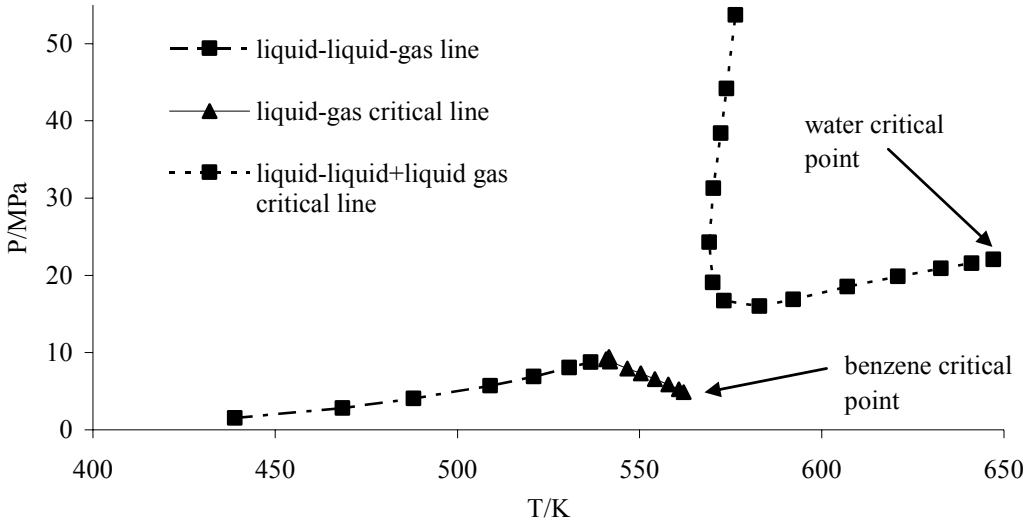

Figure 2.6: Pressure-temperature projection of mixtures of benzene and water[26].

Carbon dioxide, hydrogen[25] and n-alkanes[27] all form Type III mixtures with water. For binary mixtures of water and methane, as the mole fraction of methane increases from 0 to 0.3 the mixture critical pressure increases to 250 MPa as shown in Figure 2.7.[28] Carbon dioxide and water behave in a similar manner, as shown in Figure 2.8.[23] Hydrogen and water's pressure-temperature projection is nearly asymptotic around the critical point of water.[25] As the mole fraction of hydrogen in water increases from zero, the mixture critical pressure rapidly increases, Figure 2.9.[29]

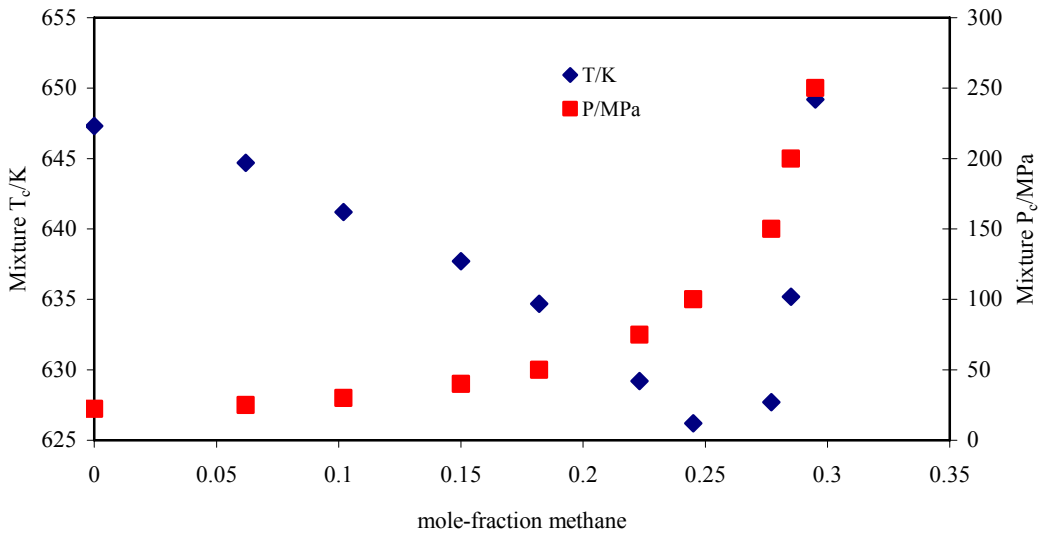

Figure 2.7: Experimentally determined critical temperature and pressure of mixtures of methane and water[28].

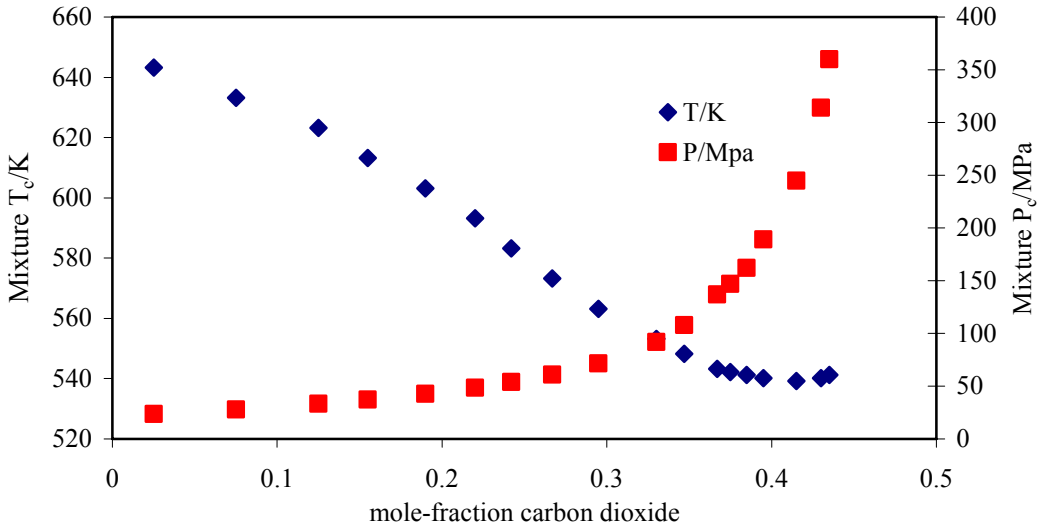

Figure 2.8: Experimentally determined critical temperature and pressure of mixtures of carbon dioxide and water[23].

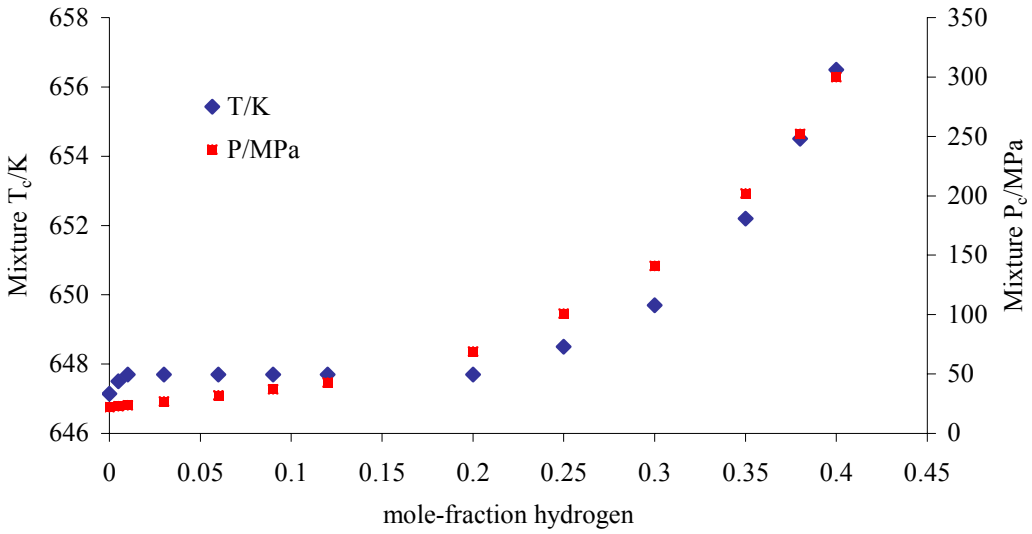

Figure 2.9: Experimentally determined critical temperature and pressure of mixtures of hydrogen and water[29].

2.3.4 Estimation of the Critical Locus of Water-Mixtures

In the absence of experimental data, another means of verifying that a mixture is truly supercritical is by determining the thermodynamic stability of the mixture at a given temperature, pressure, and composition by an iterative means using an equation of state. Thermodynamic stability is whether a mixture is in one phase—liquid, vapor, or supercritical fluid—versus being a mixture of solids, liquids, and/or gases. Critical pressure and temperature curves for binary mixtures of water and ethanol were determined using an adaptation of a computational strategy presented by Heidemann and Khalil.[30] For a fluid to be in one phase the following condition must be satisfied:

$$D = \left[A - A_0 + P_0(V - V_0) - \sum_i \mu_{i0}(n_i - n_{i0}) \right]_{T_0} > 0 \qquad (2.9)$$

where D is the tangential plane distance, A is the Helmholtz free energy, P is pressure, V is volume, μ is chemical potential, and n is the number of moles. The subscript 0 denotes

the initial condition prior to an isothermal change. Expanding this expression with respect to the Helmholtz free energy yields:

$$(D)_{T_0,V_0} = \frac{1}{2!}\sum_i\sum_j\left(\frac{\partial^2 A}{\partial n_i \partial n_j}\right)_{n_0}\Delta n_i \Delta n_j + \frac{1}{3!}\sum_i\sum_j\sum_k\left(\frac{\partial^3 A}{\partial n_i \partial n_j \partial n_k}\right)_{n_0}\Delta n_i \Delta n_j \Delta n_k + \ldots O\left(\Delta n^4\right) > 0 \tag{2.10}$$

For a mixture to be thermodynamically stable in the supercritical region, the first two expressions involving the Helmholtz free energy must be zero. This is accomplished by evaluating the following two criteria:

Criteria 1: $$b = \frac{1}{2} Q \cdot \Delta n = 0 \tag{2.11}$$

Criteria 2: $$c = \frac{1}{6}\sum_i\sum_j\sum_k\left[\frac{\partial^3 (A/RT)}{\partial n_i \partial n_j \partial n_k}\right]_{n_0}\Delta n_i \Delta n_j \Delta n_k = 0 \tag{2.12}$$

where **Q** is an N_c x N_c square matrix of the second partial derivatives of the Helmholtz free energy with respect to the numbers of moles. N_c is the total number of components in the mixture. When the determinant of **Q** is zero, the first criterion for thermodynamic stability is met. While mathematically there are several values that can satisfy criteria 1, criteria 2 allows for a refinement of criterion 1 and eventually leads to only one set of critical values. For the purposes of mixtures of ethanol and water, it is not necessary to evaluate criterion 2, since criterion 1 provided only one set of sensible values.

The elements of the matrix **Q** can be expressed by evaluating the first partial derivative of the natural logarithm of the fugacity of a component with respect to the number of moles:

$$Q_{ij} = \left[\frac{\partial^2 (A/RT)}{\partial n_i \partial n_j} \right]_{n_0} = n_T \left(\frac{\partial \ln f_i}{\partial n_j} \right) \tag{2.13}$$

The fugacity and its derivative can be found using an equation of state. For the mixture of ethanol and water, the Redlich-Kwong-Soave equation of state is used:

$$P = \frac{RT}{\upsilon - b} - \frac{a}{\upsilon(\upsilon + b)} \tag{2.14}$$

where the covolume of the mixture b is

$$b = 0.08664 \frac{RT_c}{P_c} \tag{2.15}$$

and the attractive interaction parameter a is

$$a = 0.42748 \frac{R^2 T_c^2}{P_c} F(T) \tag{2.16}$$

and

$$F(T) = \left[1 + m\left(1 - \sqrt{T/T_c}\right) \right]^2 \tag{2.17}$$

$$m = 0.480 + 1.574\omega - 0.176\omega^2 \tag{2.18}$$

R is the universal gas law constant, υ is the molar volume, T_c is the critical temperature of a pure component, P_c is the critical pressure of a pure component, and ω is the accentric factor for a pure component. For a mixture, the following mixing rules are used:

$$a = \sum_j \sum_i y_i y_j a_{ij} \tag{2.19}$$

$$b = \sum_j \sum_i y_i y_j b_{ij} \tag{2.20}$$

where y is the mole fraction of component i or j. For i=j, the value for the covolume and attractive interaction parameter of a pure component is used. For i≠j, the following mixing rules are used:

$$a_{ij} = \left(1 - k_{ij}\right)\sqrt{a_{ii}a_{jj}} \tag{2.21}$$

$$b_{ij} = \left(b_{ii} + b_{jj}\right)/2 \tag{2.22}$$

where k_{ij} is a binary interaction parameter characteristic of the equation of state of the mixture of two components. The partial derivative for the fugacity can be evaluated using

$$n_T\left(\frac{\partial \ln f_i}{\partial n_j}\right) = \frac{\delta_{ij}}{y_i} + \frac{2b_{ij}}{\upsilon - b} + \frac{\beta_i\beta_j}{(\upsilon - b)^2} + \frac{a\beta_i\beta_j}{RTb}\cdot\frac{1}{(\upsilon + b)^2} + \frac{B_1}{RTb^2}\frac{1}{(\upsilon + b)} + \frac{B_2}{RTb^3}\ln\left(\frac{\upsilon + b}{\upsilon}\right) \tag{2.23}$$

where δ_{ij} is the Kronecker delta: $\delta_{ij}=1$ if i=j and $\delta_{ij}=0$ if i≠j. In addition

$$\beta_i = 2\left(\sum_j y_j b_{ij}\right) - b \tag{2.24}$$

$$B_1 = 2a\beta_i\beta_j - b\left(\alpha_i\beta_j + \alpha_j\beta_i + a\gamma_{ij}\right) \tag{2.25}$$

$$B_2 = -B_1 - 2a_{ij}b^2 \tag{2.26}$$

and

$$\alpha_i = 2\sum_j y_j a_{ij} \tag{2.27}$$

$$\gamma_{ij} = 2b_{ij} - \beta_i - \beta_j \tag{2.28}$$

The above system of equations, along with the determinant of **Q** may be solved using a spreadsheet. The molar volume at the critical point of a mixture is approximated as 4 times the covolume of the mixture, b. An iterative scheme is used to determine the temperature at which the determinant of **Q** is zero. The initial guess for the temperature is

$$T_{initial} = 1.5 \sum_{i=1}^{n} y_i T_{ci} \tag{2.29}$$

Once a critical temperature for a mixture is computed, the critical pressure is calculated using an equation of state. The mixture critical temperature and pressure are then compared against the pure components critical properties and are also checked to insure that both values are positive.

Figures 2.10 and 2.11 are the computed critical pressure and temperature curves for ethanol and water mixtures. The estimated critical data accurately model the published data with a median error of 1.02% for the critical temperature and 1.60% for the critical pressure.

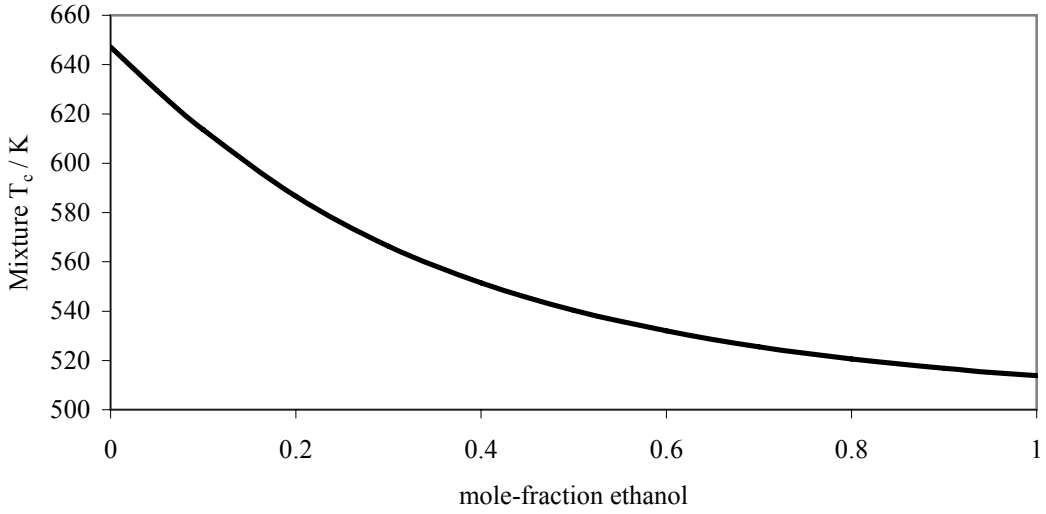

Figure 2.10: Computationally determined critical temperature curve for a mixture of ethanol and water.

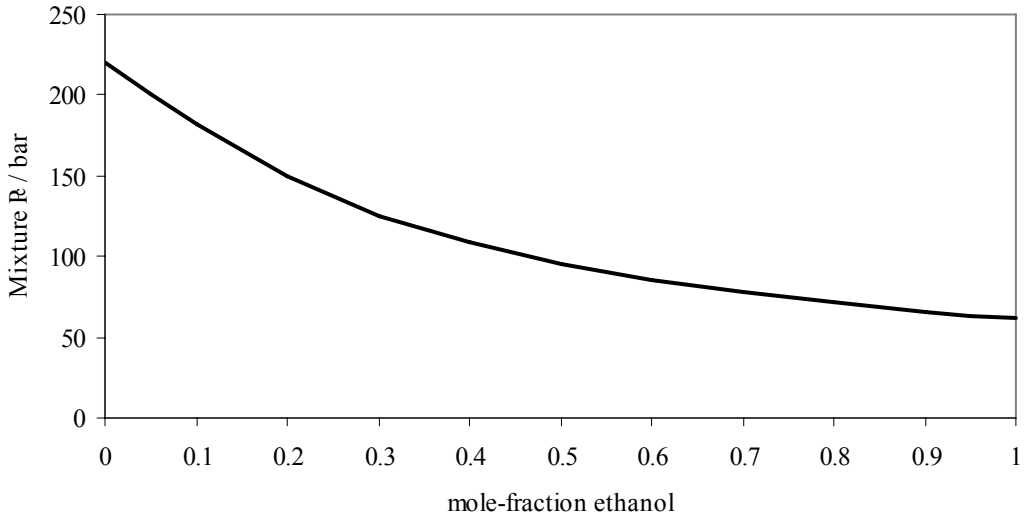

Figure 2.11: Computationally determined critical pressure curve for a mixture of ethanol and water.

2.4 Inconel as a Reactor Material for Supercritical Water Reformation

Inconel® 625 alloy has been used as a reactor body for supercritical water reformation and supercritical water oxidation for a variety of compounds, including methanol, ethanol, diesel, and military logistic fuel (JP-8).[5, 6, 31-33] The composition of Inconel® 625 is listed in Table 2.2.

Table 2.2: Limiting chemical composition of Inconel® 625.[34]

Species	%	
Nickel	58.0	Min
Chromium	20.0-23.0	
Iron	5.0	Max
Molybdenum	8.0-10.0	
Niobium (plus Tantalum)	3.15-4.15	
Carbon	0.10	Max
Manganese	0.50	Max
Silicon	0.50	Max
Phosphorus	0.015	Max
Sulfur	0.015	Max
Aluminum	0.40	Max
Titanium	0.40	Max
Cobalt	1.0	Max

Inconel® 625 is an excellent material of construction for supercritical water oxidation reactors due to its strength and chemical resistance. Inconel® 625 is resistant to corrosion in marine environments, chemical attack from nitric and hydrochloric acids, and oxidation at high temperatures. In addition, at a temperature of 650°C it has a high tensile strength of approximately 820 MPa and a high yield strength of approximately 410 MPa.[34]

At ambient conditions, the surface of an Inconel® 625 reactor body is mostly oxides of nickel, chromium, and molybdenum. However, supercritical water environments change the surface chemical composition of Inconel® 625. Kritzer et. al.

performed a series of experiments to determine the effects of supercritical water oxidation on Inconel® 625. Their reactor was 1000 mm in length with an inner diameter of 8.5 mm. An 800 hour experiment was performed at 500°C and 24 MPa using a hydrogen peroxide solution as a feedstock. The solution feed rate was 1 g/min with a resultant oxygen concentration of 1.44 mol/kg. At these conditions, nickel, chromium, and molybdenum were found in the reactor effluent at concentrations of 0.5 ppm, 1.7 ppm, and 0.6 ppm respectively. The estimated corrosion rate of the reactor wall was 0.06 μm/hr. [33]

Boukis et. al. studied the catalytic role of Inconel® 625 as a reactor material in supercritical water reformation of methanol.[31] After operating an Inconel® 625 reactor for 1000 hours at 625°C, the reactor surface was examined using a scanning electron microscope with an energy dispersive x-ray spectrometer (SEM/EDX). The reactor surface was found to be composed of grains approximately 1 μm in diameter with a composition of 93 wt-% nickel. The three-dimensional surface area of the reactor was 1.2 times larger than the two-dimensional surface area. The main effect was enhanced catalytic activity caused by the reactor surface influencing the forward water-gas shift reaction.

CHAPTER 3

EXPERIMENTAL METHODOLOGY

3.1 Materials Used

The ethanol used for this work was undenatured ethanol, 95% ethanol and 5% water by volume, from Pharmoco-Aaper obtained through the University of Missouri—Columbia Chemstores. The water used for this work was distilled and deionized. The carrier gas for the gas chromatograph was Ultra Pure Carrier Grade (UPC 5.5) Argon with a purity of 99.9995% from Airgas.

3.2 Experimental Apparatus

Figure 3.1 is a representative process flow diagram of the system used for this work. The experimental apparatus consists of four different process sections:

1. Feed System
2. Heat Recovery and Feed Preheat
3. Supercritical Water Reactor (SWR)
4. Sample Collection and Analysis

3.2.1 Feed System

The feed system consists of water and fuel storage, balances, and two pumps. Water and ethanol are stored in separate five-gallon high-density polyethylene jugs resting on balances. The balances are used to determine the mass flow rate of water and ethanol during an experiment. The water balance was manufactured by Arlyn Scales, model number 610C, with a range of 0-46 kg with reading increments of 0.01 kg. The fuel balance was also manufactured by Arlyn Scales, model number D620L, with a range of 0-22,000 g with reading increments of 2 g. The two pumps were micrometering piston pumps

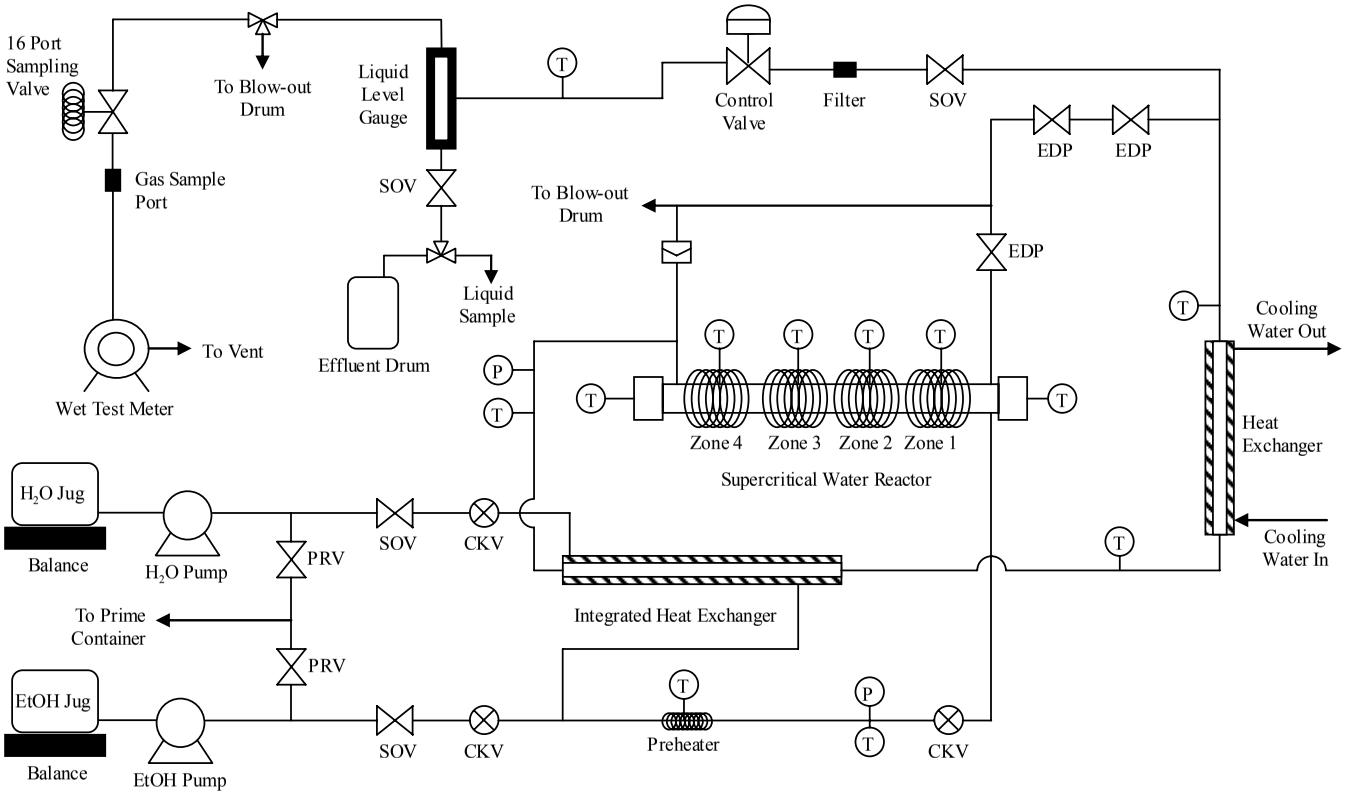

Figure 3.1: A representative process flow diagram for the supercritical water reforming section of the MU hydrogen reforming unit.

manufactured by Eldex Laboratories. The ethanol pump is capable of delivering between 0.1 and 10 mL/min of liquid up to a maximum pressure of 5000 psig. The water pump is capable of delivering between 0.1 and 100 mL/min of liquid up to a maximum pressure of 5000 psig. The calibration fluid used by Eldex for the pumps' flow specifications was isopropyl alcohol. The downstream lines for the pumps were 1/4" outer diameter (OD) seamless 316 stainless steel tubing.

The pumps are primed by opening the prime valves (PRV) to allow fluid to flow through the pumps at ambient pressure. The pumps may be isolated from the remainder of the experimental apparatus by regulated tee shut-off valves (SOV), which are redundantly protected by poppet-style check valves (CKV).

3.2.2 Heat Recovery and Preheat

In order to recover heat from the reactor effluent, the feed water and reactor effluent pass through an integrated heat exchanger. The integrated heat exchanger is a double-pipe heat exchanger with the reactor effluent passing through the inner tube and feed water passing through the outer tube. Due to concerns about corrosion and pitting from supercritical effluent entering the heat exchanger, the inner tube is ¼" OD heavy-wall (0.065" wall thickness) seamless Hastelloy® C276 tubing. The outer tube is ½" OD 316 stainless steel.

After the feed water passes through the integrated heat exchanger, it mixes with the fuel and passes through the preheater. The preheater is constructed of ¼" OD heavy-wall seamless Hastelloy® C276 tubing with electrical heat tape wrapped around the exterior of the tubing. The heat tape uses 110 volts AC and is protected by a 15 amp

breaker. The heat tape is controlled by Labview software and a solid state relay on a thirty-second cycle. A thermocouple measures the outer wall temperature, which is not allowed to exceed 500°C. The inlet thermocouple is the controlling thermocouple for the heat tape.

The reactor effluent that passes through the integrated heat exchanger then passes through a second double-pipe heat exchanger constructed of 316 stainless steel tubing. The second heat exchanger is cooled by tap water. After the reactor effluent passes through both heat exchangers, it then passes through a strainer and particulate filter, followed by a control valve. The control valve is a Badger Meter, Inc. Research Control Valve which is pneumatically actuated and computer controlled. The control valve body is constructed of Hastelloy® C276 with a Stellite trim set. The control valve regulates the pressure in the Supercritical Water Reactor (SWR), with the SWR inlet pressure being the control variable.

3.2.3 Supercritical Water Reactor

The supercritical water reactor is a custom-designed tubular reactor with an internal volume of approximately 56.5 in^3, or 0.926 liters. The reactor has an inner diameter of 1.00 in, an outer diameter of 1.75 in, and an internal length of 71.50 in. The SWR was manufactured by the Parr Instrument Company and is made of Inconel® 625 Grade 1 alloy, mounted at a 13° angle inside the experimental apparatus's enclosure. The SWR is ASME rated at 5000 psig at 650°C. The gasket material used at the reactor head sealing surface is grafoil. The reactor has ports on the sides near the heads that serve as reactant inlet and effluent outlet ports. Preheated reactants are feed at the lower end of the

reactor, and the effluent flows out of the upper end of the reactor. Figure 3.2 shows the dimensions of the reactor tube without the heads attached.

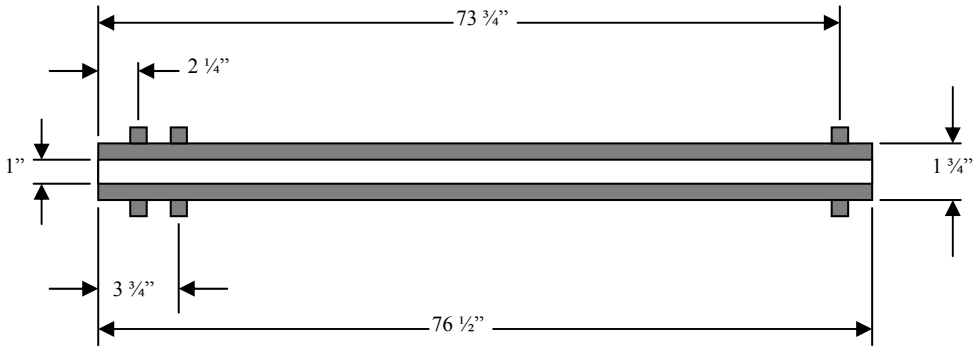

Figure 3.2: Dimensions of the Inconel 625 Grade 1 supercritical water reactor.

Two thermowells, also constructed of Inconel® 625 Grade 1, extend from the reactor heads to the center of the reactor. Four Type K thermocouples (RTC) were placed along the length inside each thermowell at positions illustrated in Figure 3.3. The SWR is heated by a four zone radiant clam-shell shaped heater manufactured by Watlow Electric Manufacturing Company. Each zone consists of two elements, each of which are rated at 1000 watts at 120 volts. Each zone is operated at 208 volts with a maximum heater duty of 1502 watts per zone. Each zone is protected by a 15 amp breaker.

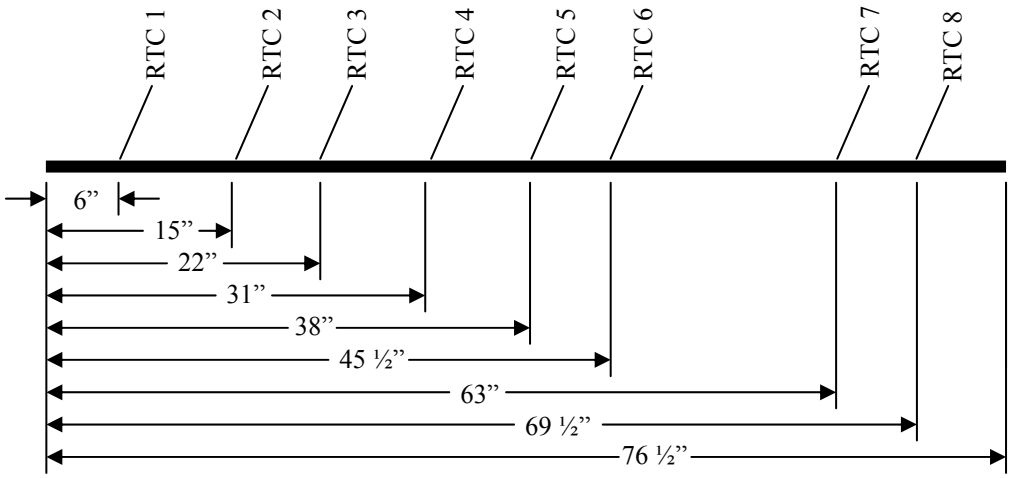

Figure 3.3: Thermocouple placement in the SWR.

Each heater zone has redundant Type K thermocouples (zone thermocouples) monitoring the reactor outer-skin temperature at the mid-point of the length of each heating zone. The SWR skin temperature is not allowed to exceed 750°C due to the material properties of Inconel® 625. The SWR heaters are proportionally controlled by Labview software using solid state relays on a thirty-second cycle with a proportional control constant of 4. The thermowell thermocouples provide the signal that acts as the control variable. A four-zone Omega Engineers Controller provides back-up SWR heater control for the Labview control software to prevent overheating the reactor. SWR thermowell thermocouples RTC 3, RTC 4, RTC 6, and RTC 7 are the controlling thermocouples for SWR Heater Zones 1, 2, 3, and 4, respectively.

Several safety features protect the SWR from overheating and over-pressurization. First, the Labview software will turn off the appropriate zone heater if the SWR skin temperature exceeds 750°C. In addition, if there is a failure of the data acquisition and control system, an Omega Four Zone controller will turn off the

appropriate zone heater if the SWR skin temperature exceeds 760°C. In addition, the Labview software will turn off the SWR heaters, the water pump, and the fuel pump if the SWR inlet pressure exceeds 50 psig above the set-point. The SWR pressure set-point is software limited to a maximum of 5000 psig.

In addition, there are two operator means of depressurizing the SWR in addition to using the Labview data acquisition and control system. The SWR can be depressurized using an emergency depressurization valve (EDP) at either the reactor inlet or the outlet. The reactor outlet has two EDP valves in series in order to maintain reactor pressure in the event that one of the valve's seats begins to fail. The reactor is also protected from over-pressurization by a temperature and pressure-rated Inconel 625 rupture disc in a safety head assembly at the SWR exit.

3.2.4. Sampling

For this investigation, two different samples were collected, either gas samples or liquid samples. After the reactor effluent undergoes an expansion at the control valve, the gas/liquid mixture is disentrained in a Strahman Sight Gauge (liquid reservoir or LR1). The liquid level in the gauge is operator monitored and must be periodically drained by opening a shutoff valve (SOV). The liquid effluent is then either collected in a 5-gallon high density polyethylene jug for disposal or in a sample container for further analysis.

The gaseous effluent from the SWR flows through LR1 and into the gas sampling system, which consists of a bypass line to vent, a 16-port Valco multisample valve, a gas chromatograph (GC) gas sample syringe port, and a wet-test meter. The 16-port sampling valve allows for gas samples to be collected over time and analyzed at a time of

convenience. The gas sample syringe port allows for immediate sampling of the gaseous effluent for GC analysis. The wet-test meter is used to determine the gas effluent's volumetric flow-rate over time.

3.3 General Procedure

3.3.1 Operating Procedure

The generalized procedure may be divided into the following: Cold Start-up Procedure, Experimental Data Collection, Change of Experimental Run Conditions, and Shutdown.

To perform an experimental run, the preheater, the integrated heat exchanger, and supercritical water reactor must be thermally stable. Since the effluent from the SWR is used to provide part of the thermal energy to heat the feed water, the current experimental apparatus can take a couple of hours to become thermally stable. In order to bring the SWR up to operating temperature and pressure, the following steps must occur:

1. All valve positions must be noted, the SWR outlet valve should be open and the remainder of valves closed.
2. The Data Acquisition and Control System needs to be turned on and the operating conditions entered.
3. The SWR Zone Heaters need to be turned on to bring the SWR up to operating temperature. The preheater should also be turned on.
4. Once the SWR is nearing operating temperature, the water pump should be primed and water shut-off valve opened and the reactor pressurized with water. (Note: Running the pumps with shut-off valves closed will damage the pumps)
5. Once the SWR is nearing operating pressure, supercritical water will begin flowing through the integrated heat exchanger. The liquid level gauge must now be checked periodically and drained to prevent it from overfilling.

At this point, the SWR will begin to reach a thermally stable point. The inlet temperature of the SWR will begin to increase and then stabilize. The exit temperature of the reactor effluent side of the integrated heat exchanger will also begin to increase and then

stabilize. Once the SWR inlet temperature and integrated heat exchanger temperature has stabilized, the experimental apparatus is ready for ethanol to be fed in.

The experimental start time is considered to be when the fuel pump is turned on and the fuel, ethanol, is pumped into the reactor. Depending on the experimental run's residence time, the production of gaseous effluent should reach a steady flow-rate half an hour after the fuel is first fed to the reactor. The evidence of gas production is noted as an increase in pressure in the liquid level reservoir and also by movement of the face dial of the wet-test meter. During an experiment, the following are performed:

1. Every quarter hour the masses shown on the water and ethanol balances are noted in the lab notebook.
2. At 30-minute intervals, a gas sample is taken using the gas sample syringe and injected into the GC.
3. At the mid-point and end of a run, a gas sample is taken using the 16-port gas sample valve.
4. At the mid-point and near the end of the run, the liquid reservoir is completely emptied, the time noted, and it is allowed to refill. Once the liquid level reaches the top of the reservoir, the liquid is drained into a sample bottle, and the time noted.
5. Periodically, the gas flow-rate is measured using the wet-test meter.

Using this procedure, an experimental run will last approximately 90 minutes. At the conclusion of an experimental run, the fuel pump is turned off. The reactor can then be shut-down by a step-wise procedure or prepared for another experiment. If another experiment is performed, the new experimental flow-rates, temperature, and pressure are set, and after 60 minutes the system is typically thermally stable and another experiment can be performed.

To shut-down the SWR, the SWR zone heaters and the preheater are turned off. Water is fed into the reactor for thirty minutes, and then the reactor is slowly depressurized. Once the SWR pressure reaches 250 psig, the SWR outlet emergency

depressurization valves are opened and the reactor is allowed to cool. It is important to note that the SWR outlet EDP valves must remain open while the reactor cools or otherwise the pressure in the reactor will fall below atmospheric pressure, and the pressure transducers can be damaged.

3.3.2 Selection of Experimental Conditions

The experimental conditions selected for this work were based on supercritical fluid properties, equipment limitations, and literature reviews. The experimental conditions to consider include reactant concentrations, reactant feed rates, temperature, and pressure.

For this work, the minimum pressure and temperature are bounded by the critical point of water, P_c=22.4 MPa and T_c=374°C. The upper bounds for temperature and pressure are limited by the design and material of construction of the supercritical water reactor, which is ASME Rated at 34.6 MPa at 650°C. The supercritical water reactor may be operated at temperatures above 650°C, but at reduced pressures inasmuch as the tensile strength of the reactor body decreases with increasing temperature.[32] The maximum temperature at which the current supercritical water reactor may be safely operated is 710°C interior temperature at 24.2 MPa.

For future potential process commercialization, it is of interest to attempt to convert all ethanol fed into the reactor into products that would remain gaseous at ambient conditions, preferably hydrogen and carbon dioxide. Since previously published work indicates that the presence of acetaldehyde appears to be non-existent above 600°C in a catalytic system, a temperature range between 630°C and the reactor maximum of 710°C was chosen for this investigation, even though the process of interest is

noncatalytic. The operating pressure for this work was fixed at 24.2 MPa to allow for operation at the reactor's maximum temperature, 710°C, and to speed thermal stabilization between experimental runs.

Water and ethanol flow rates are both limited by the balances, pumps, reactor thermal stability, and the control valve. The fuel balance/pump combination can reproducibly operate at a mass flow rate of no less than 0.25 g/min, since the fuel balance reads in 2-gram increments. At flow rates less than 0.25 g/min, it takes a considerable amount of time to determine if the pump is functioning or malfunctioning. The fuel pump has an upper bound of 10 g/min. Likewise, the water pump cannot be operated reproducibly at mass flow rates below 6 g/min and is bounded by a maximum flow of 100 g/min.

When considering thermal stability and pressure control, the current reactor operates best with water flow rates of less than 20 g/min. At flow rates greater than 20 g/min, it is difficult to achieve thermal uniformity along the length of the reactor. If coking reactions occur, lower flow rates of water and fuel are desirable to maximize run-time without clogging the reactor. It is also desirable to keep ethanol flow rates low in comparison with water, as it has been theorized that greater steam to carbon ratios result in higher conversion of ethanol to hydrogen and carbon dioxide[35].

3.3.3 Design of Experiments

The design of experiments for this work was chosen to determine the main and interactive effects of temperature, ethanol concentration, and space time upon the kinetics of ethanol reformation to hydrogen, carbon oxides, and hydrocarbons while keeping the

pressure of the system fixed. For this work, a central composite circumscribed design of experiments with a 2^3 factorial portion and three center points was chosen.[36] The order in which the experiments are to be performed was randomized. The test variables are reactor temperature, ethanol flow rate, and water flow rate. The experimental design is shown in Table 3.1.

Table 3.1: Design of experiments in coded and uncoded variables

DOE	Experimental	Coded Variables			T /	EtOH /	H_2O /
Line	Order	X1	X2	X3	°C	$g \cdot min^{-1}$	$g \cdot min^{-1}$
1	9	-1	-1	-1	650	0.625	9
2	10	+1	-1	-1	690	0.625	9
3	4	-1	+1	-1	650	1.375	9
4	16	+1	+1	-1	690	1.375	9
5	17	-1	-1	+1	650	0.625	15
6	12	+1	-1	+1	690	0.625	15
7	5	-1	+1	+1	650	1.375	15
8	2	+1	+1	+1	690	1.375	15
9	15	0	0	0	670	1	12
10	7	0	0	0	670	1	12
11	3	0	0	0	670	1	12
12	6	-2	0	0	630	1	12
13	1	+2	0	0	710	1	12
14	14	0	-2	0	670	0.25	12
15	11	0	+2	0	670	1.75	12
16	13	0	0	-2	670	1	6
17	8	0	0	+2	670	1	18

3.3 Product Characterization

The gas samples collected for this study were analyzed using a Hewlett-Packard 5890 Series A Gas Chromatograph equipped with a thermal conductivity detector (TCD). GC data were collected and integrated using HP Chemstation® Software version A.06.03 build 509. Argon was chosen as the carrier gas over helium to allow for better detection of hydrogen gas and to avoid multiple inversions of the TCD signal.[37] The column was manufactured by Supelco, part number 1-2392-U, and is 15 feet long, 1/8 inch in diameter and constructed of stainless steel. The column packing is 60/80 Carboxen®

1000, lot number 021599. The column packing is designed to detect permanent gases and can be used to distinguish between hydrogen, nitrogen, oxygen, carbon monoxide, methane, carbon dioxide, acetylene, ethylene, ethane, and propane.

Three different methods were used for GC analysis. Methods Air02 and Air03 were used for gas samples injected into the GC using a gas sample syringe. Method Loop05 was used for gas sample loops injected into the GC. Method Air02 is a fast method capable of detecting hydrogen, nitrogen, oxygen, carbon monoxide, methane, and carbon dioxide. Method Air02 is used for the first two gas syringe samples taken during an experimental run. Method Air03 and Loop05 can detect all the gases from Method Air02 and in addition can detect ethylene and ethane. Method Air03 is the method used for the last gas syringe sample taken in a run. The parameters for each method are listed in Table 3.2.

Table 3.2: Parameters for each GC method.

Method	**Air02**	**Air03**	**Loop05**
Inlet Temperature / °C	120	120	120
TCD Temperature / °C	220	220	220
Oven Maximum / °C	200	200	200
Oven Equilibrium Time / min	3	3	3
Initial Oven Temperature / °C	40	40	40
Initial Oven Time / min	8	8	10
Ramp 1 Rate / °C·min^{-1}	20	20	8
Ramp 1 Final Temperature / °C	140	140	140
Ramp 1 Hold Time / min	8.5	7	7.5
Ramp 2 Rate / °C·min^{-1}	N/A	20	10
Ramp 2 Final Temperature / °C	N/A	200	200
Ramp 2 Hold Time / min	N/A	16.5	13
Method Duration / min	21.5	39.5	49

Experimental run gas samples were injected using a Hamilton Gastight® model 1001 stop-cocked gas syringe. The injected gas volume was 1.0 mL. The injected gas volume from the Valco 16-port multi-sampling valve was also 1.0 mL.

The GC was calibrated by injecting different volumes of neat hydrogen, oxygen, nitrogen, methane, carbon dioxide, and carbon monoxide. All neat calibration gasses had a purity of at least 99%. The GC was also calibrated by injecting different volumes of pure gases and various gas mixtures. Neat gases used for calibration were from Airgas and were Hydrogen 2.0, Methane 2.0, Nitrogen 2.0, Oxygen 2.0, and Carbon Dioxide 4.0. Gas mixtures used for calibration were in-house blended mixtures of pure gases from Airgas and purchased calibration mixtures from Supelco. The first purchased gas mixture, Supelco catalog number 501743, was 14.97% carbon dioxide, 6.99% carbon monoxide, 4.50% methane, 4.00% oxygen, with the balance being nitrogen. All compositional values are in mole percents, and the accuracy of the manufacturer's gas analysis was ±5%. The second purchased gas mixture, Supelco catalog number 23462, was 1.00% acetylene, 1.00% carbon dioxide, 1.00% carbon monoxide, 1.02% ethane, 1.00% ethylene, 0.999% methane, with the balance being nitrogen. The accuracy of the manufacturer's gas analysis is ±2%. The retention order and typical retention times for each calibration gas are listed in Table 3.3. GC calibration data and calibration curves are presented in the appendix.

Table 3.3: Retention time for each calibrated species using a syringe or sample loop.

Retention Order	Species	Retention Time GSS /min	Retention Time GSL /min
1	Hydrogen	2.5	3.4
2	Nitrogen	5.5	6.5
3	Carbon Monoxide	7.2	8.4
4	Methane	12.1	15.9
5	Carbon Dioxide	16.3	22.2
6	Ethylene	24.8	35.0
7	Ethane	29.0	39.1

CHAPTER 4

RESULTS AND DISCUSSION

4.1 Experimental Results and Material Balance

The seventeen supercritical water reformation experiments of ethanol were conducted over a four day period, 31 hours of which ethanol was fed into the reactor. A total of 4.968 kg of 95% ethanol was fed into the reactor and 18.81 kg of water. The target and observed operating conditions are listed in Table 4.1.

Table 4.1: Target and observed experimental temperature, flow rates, and pressure

		Targets				Observed			
Run ID	DOE Line	T/ K	EtOH / $g \cdot min^{-1}$	H_2O / $g \cdot min^{-1}$	P/ MPa	T/ K	EtOH / $g \cdot min^{-1}$	H_2O / $g \cdot min^{-1}$	P/ MPa
A	13	983	1.000	12	24.20	982.9	0.93	11.4	24.21
B	8	963	1.375	15	24.20	966.6	1.55	16.1	24.22
C	11	943	1.000	12	24.20	944.2	0.90	11.4	24.20
D	3	923	1.375	9	24.20	930.3	1.55	9.2	24.19
E	7	923	1.375	15	24.20	930.3	1.55	14.1	24.20
F	12	903	1.000	12	24.20	901.4	0.91	11.3	24.18
G	10	943	1.000	12	24.20	944.0	0.92	11.4	23.83
H	17	943	1.000	18	24.20	941.3	0.90	19.7	24.18
I	1	923	0.625	9	24.20	930.7	0.52	9.3	23.96
J	2	963	0.625	9	24.20	966.5	0.61	9.3	24.24
K	15	943	1.750	12	24.20	943.2	2.02	11.3	24.23
L	6	963	0.625	15	24.20	964.3	0.58	13.7	24.24
M	16	943	1.000	6	24.20	944.1	0.91	6.4	23.98
N	14	943	0.250	12	24.20	943.7	0.17	11.5	24.19
O	9	943	1.000	12	24.20	943.6	0.93	11.6	24.18
P	4	963	1.375	9	24.20	966.6	1.55	9.3	24.20
Q	5	923	0.625	15	24.20	929.1	0.59	13.6	24.30

The observed temperature is the mean of the temperatures measured by reactor thermocouples (RTC) 3, 4, 5, 6, and 7 over the period of the experimental run. The temperature was measured at half-second intervals. Temperatures measured by RTC 1 and RTC 8 were not included in the average, since these thermocouples measure the

temperature of the reactor heads, which are not heated. RTC 2 measures the reactor temperature near the inlet of the reactor, where the reactants are being heated to experimental temperature. RTC 2 temperatures are likewise omitted from the average reactor temperature. The pressure is the mean pressure measured over the period of the experiment at the reactor inlet. The average temperature measured by each reactor thermocouple and the average pressure measured at the inlet and outlet of reactor for each run are listed in Table A.9 in the appendix.

At fifteen minute intervals and at the beginning and end of an experimental run, the masses of the ethanol and water jugs were recorded. The observed ethanol and water mass flow rates were calculated by dividing the change in mass between the beginning and the end of a run by the experimental run time. The ethanol and water jug masses at the beginning and end of each run as well as the duration of each run are listed in Table A.10 in the appendix.

For each experiment, multiple wet-test meter measurements were conducted, liquid effluent samples were collected, and gas effluent samples were sampled and analyzed. Table 4.2 shows the average liquid and gaseous effluent rates from the reactor for each experimental run as well as the gaseous effluent composition. Table A.11 in the appendix lists each wet-test meter measurement of the gas effluent rate. The liquid effluent rate data are in Table A.12, which is also in the appendix. The liquid effluent collected averaged a total carbon content of 10 ppm. The gas effluent was analyzed using Hewlett Packard ChemStation software, which generated the integrated peak areas of each species in a gas sample. Using a linear regression of the GC calibration data (Figures A.2-A.6 in the appendix) and the integrated peak areas, the molar quantity of

each species in a gas sample was calculated. The integrated peak areas for each gas sample are in Tables A.7 and A.8 in the appendix.

Table 4.2: Ambient condition gas and liquid effluent rates and gas effluent mole fractions

	Effluent Rates		Outlet Gas Mole fractions				
Run ID	Gas / $L \cdot min^{-1}$	Liquid / $g \cdot min^{-1}$	H_2 / mol-%	CO / mol-%	CH_4 / mol-%	CO_2 / mol-%	C_2H_6 / mol-%
A	2.19	11.23	53.4%	1.6%	18.3%	23.3%	0.2%
B	3.52	17.12	53.0%	1.6%	19.9%	23.4%	1.8%
C	2.02	10.75	52.8%	1.0%	19.8%	23.8%	2.1%
D	3.19	8.85	49.7%	2.4%	22.8%	23.2%	3.0%
E	3.22	14.49	51.5%	1.5%	21.0%	23.7%	2.7%
F	2.13	10.74	54.1%	0.6%	18.9%	24.0%	1.7%
G	2.06	10.97	52.6%	0.7%	20.6%	24.3%	2.2%
H	2.16	17.80	54.1%	0.7%	18.4%	23.8%	2.2%
I	1.18	9.04	53.1%	0.4%	19.7%	22.5%	2.1%
J	1.44	11.06	58.2%	0.5%	16.8%	22.4%	1.6%
K	4.17	11.39	49.1%	1.9%	23.4%	23.1%	3.1%
L	1.42	13.45	57.4%	0.1%	18.0%	22.1%	1.6%
M	1.90	6.19	49.4%	1.3%	23.0%	22.4%	2.4%
N	0.43	11.37	60.0%	0.0%	15.1%	23.6%	1.6%
O	2.02	11.31	53.0%	0.7%	19.9%	23.6%	2.2%
P	3.20	8.95	51.0%	2.0%	23.5%	23.5%	2.0%
Q	1.35	13.52	56.1%	0.4%	19.2%	24.3%	1.8%

At the conclusion of the design matrix, the reactor was opened and inspected. The interior of the reactor was found to be free of deposits, which in turn indicates that the supercritical water reformation of ethanol at the conditions considered did not result in coking or fouling of the reactor. This coking-free inspection result as well as the low carbon content in the liquid effluent (10 ppm) indicates that ethanol was completely converted to gaseous product species. This result is also reflected in an effective closure of the atomic carbon balance in Table 4.3, based on ethanol feed and gaseous effluent.

Based on ethanol feed rates and gaseous effluent composition, an atomic balance of hydrogen and oxygen is in Table 4.4. The molar flow rates and molar fractions of the reactor feed and effluent are listed in Tables 4.5 and 4.6.

Table 4.3: Atomic carbon balance

Run ID	DOE Line	Carbon In mmol·min^{-1}	Carbon Out mmol·min^{-1}	Difference mmol·min^{-1}	Percentage Difference
A	13	39.7	38.6	-1.1	-2.8%
B	8	66.1	66.7	0.6	1.0%
C	11	38.3	38.4	0.1	0.3%
D	3	65.8	67.8	2.0	3.0%
E	7	65.7	65.1	-0.7	-1.0%
F	12	38.6	38.9	0.3	0.9%
G	10	39.1	40.3	1.2	3.0%
H	17	38.1	39.9	1.9	4.9%
I	1	22.0	21.5	-0.4	-2.0%
J	2	26.1	24.0	-2.1	-8.0%
K	15	86.0	89.1	3.0	3.5%
L	6	24.6	24.1	-0.5	-1.9%
M	16	38.8	38.3	-0.5	-1.2%
N	14	7.3	7.1	-0.2	-3.2%
O	9	39.7	38.5	-1.2	-3.1%
P	4	65.8	66.7	0.9	1.4%
Q	5	25.1	25.1	0.0	0.2%

Table 4.4: Hydrogen and oxygen from ethanol fed to the reactor, hydrogen and oxygen exiting the reactor

Run ID	DOE Line	H in mmol·min^{-1}	O in mmol·min^{-1}	H out mmol·min^{-1}	O out mmol·min^{-1}
A	13	119.1	19.9	162.3	40.6
B	8	198.2	33.0	275.6	65.4
C	11	114.9	19.1	158.3	37.6
D	3	197.5	32.9	264.4	59.7
E	7	197.2	32.9	260.9	60.3
F	12	115.7	19.3	164.3	39.5
G	10	117.4	19.6	165.0	38.9
H	17	114.2	19.0	168.1	40.1
I	1	65.9	11.0	92.6	20.5
J	2	78.3	13.0	110.5	24.9
K	15	258.1	43.0	349.2	76.9
L	6	73.7	12.3	111.5	24.2
M	16	116.3	19.4	155.2	33.5
N	14	21.9	3.6	32.7	7.8
O	9	119.1	19.9	160.1	37.1
P	4	197.4	32.9	266.1	60.4
Q	5	75.4	12.6	107.6	25.4

Table 4.5: Molar flow rates at the inlet and outlet of the reactor. Species A—ethanol, B—water, C—hydrogen, D—carbon monoxide, E—methane, F—carbon dioxide, G—ethane

		SWR Inlet Flow mol·min^{-1}		SWR Outlet Flow mol·min^{-1}					
Run ID	DOE Line	EtOH (F_{AO})	H_2O (F_{B0})	H_2O (F_B)	H_2 (F_C)	CO (F_D)	CH_4 (F_E)	CO_2 (F_F)	C_2H_6 (F_G)
A	13	0.0199	0.6354	0.6132	0.0467	0.0014	0.0160	0.0204	0.0002
B	8	0.0330	0.8964	0.8616	0.0744	0.0022	0.0279	0.0328	0.0025
C	11	0.0191	0.6338	0.6139	0.0424	0.0008	0.0159	0.0192	0.0017
D	3	0.0329	0.5106	0.4815	0.0631	0.0030	0.0289	0.0295	0.0038
E	7	0.0329	0.7839	0.7541	0.0661	0.0020	0.0270	0.0303	0.0035
F	12	0.0193	0.6301	0.6083	0.0458	0.0005	0.0160	0.0203	0.0014
G	10	0.0196	0.6338	0.6129	0.0432	0.0006	0.0169	0.0200	0.0018
H	17	0.0190	1.0953	1.0727	0.0467	0.0006	0.0159	0.0205	0.0019
I	1	0.0110	0.5187	0.5083	0.0249	0.0002	0.0092	0.0106	0.0010
J	2	0.0130	0.5188	0.5059	0.0333	0.0003	0.0096	0.0128	0.0009
K	15	0.0430	0.6314	0.5945	0.0816	0.0031	0.0389	0.0384	0.0051
L	6	0.0123	0.7593	0.7464	0.0326	0.0000	0.0102	0.0125	0.0009
M	16	0.0194	0.3587	0.3433	0.0373	0.0010	0.0174	0.0169	0.0018
N	14	0.0036	0.6399	0.6354	0.0103	0.0000	0.0026	0.0041	0.0003
O	9	0.0199	0.6425	0.6237	0.0426	0.0006	0.0160	0.0190	0.0018
P	4	0.0329	0.5198	0.4900	0.0652	0.0026	0.0301	0.0301	0.0026
Q	5	0.0126	0.7566	0.7428	0.0302	0.0002	0.0103	0.0131	0.0010

Table 4.6: Mole fractions at the inlet and outlet of the reactor. Species A—ethanol, B—water, C—hydrogen, D—carbon monoxide E—methane, F—carbon dioxide, G—ethane

Run ID	DOE Line	T/K	x_{A0}	x_{B0}	x_B	x_C	x_D	x_E	x_F	x_G
A	13	983	0.0303	0.9697	0.8787	0.0669	0.0020	0.0230	0.0292	0.0003
B	8	967	0.0355	0.9645	0.8603	0.0743	0.0022	0.0279	0.0328	0.0025
C	11	944	0.0293	0.9707	0.8848	0.0611	0.0011	0.0229	0.0276	0.0024
D	3	930	0.0606	0.9394	0.7896	0.1035	0.0050	0.0474	0.0484	0.0062
E	7	930	0.0402	0.9598	0.8541	0.0748	0.0022	0.0305	0.0344	0.0039
F	12	901	0.0297	0.9703	0.8786	0.0662	0.0007	0.0231	0.0293	0.0021
G	10	944	0.0299	0.9701	0.8814	0.0621	0.0008	0.0243	0.0287	0.0026
H	17	941	0.0171	0.9829	0.9262	0.0403	0.0005	0.0137	0.0177	0.0016
I	1	931	0.0207	0.9793	0.9172	0.0449	0.0004	0.0167	0.0191	0.0017
J	2	967	0.0245	0.9755	0.8989	0.0592	0.0005	0.0171	0.0228	0.0016
K	15	943	0.0638	0.9362	0.7807	0.1071	0.0041	0.0510	0.0504	0.0067
L	6	964	0.0159	0.9841	0.9298	0.0406	0.0000	0.0127	0.0156	0.0011
M	16	944	0.0512	0.9488	0.8218	0.0894	0.0023	0.0417	0.0405	0.0043
N	14	944	0.0057	0.9943	0.9736	0.0158	0.0000	0.0040	0.0062	0.0004
O	9	944	0.0300	0.9700	0.8863	0.0606	0.0008	0.0228	0.0270	0.0025
P	4	967	0.0595	0.9405	0.7898	0.1050	0.0042	0.0484	0.0484	0.0042
Q	5	929	0.0163	0.9837	0.9313	0.0379	0.0003	0.0130	0.0164	0.0012

In order to calculate the space time, reactant, and product concentrations, which are all important parameters for analyzing the process kinetics, the molar volume at the inlet and outlet of the reactor must be calculated. The molar volume for each experimental run was regressed by means of the Peng-Robinson-Stryjek-Vera equation of state. The temperature and inlet and outlet compositions in Table 4.6 and the pressure in Table 4.1 were used in this property estimation. With the calculated molar volume and the molar flow rates in Table 4.5, the volumetric flow rate at the inlet is calculated. Given the volume of the reactor, the space time for each experimental run condition may be determined. The molar volume, volumetric flow rate, and space time are listed in Table 4.7. The concentrations of each species at the inlet and outlet of the reactor are listed in Table 4.8.

Table 4.7: Molar volume, volumetric flow rate, and space time

			Inlet			Outlet	
Run ID	DOE Line	T / K	V_m / $cm^3 \cdot mol^{-1}$	Q / $cm^3 \cdot min^{-1}$	τ / s	V_m / $cm^3 \cdot mol^{-1}$	Q / $cm^3 \cdot min^{-1}$
A	13	983	316.0	207.0	268	322.9	225.8
B	8	967	308.7	286.9	194	316.8	317.6
C	11	944	298.2	194.7	285	305.7	212.3
D	3	930	293.3	159.4	348	305.8	186.8
E	7	930	292.2	238.7	233	301.5	266.6
F	12	901	278.0	180.5	308	287.1	199.0
G	10	944	303.1	198.0	281	310.7	216.3
H	17	941	296.5	330.4	168	301.8	349.9
I	1	931	294.6	156.0	356	300.6	166.7
J	2	967	307.8	163.7	339	314.1	176.9
K	15	943	299.1	201.7	275	311.3	237.5
L	6	964	306.3	236.3	235	311.1	249.9
M	16	944	302.2	114.3	486	312.6	130.8
N	14	944	296.9	191.1	291	299.5	195.5
O	9	944	298.2	197.5	281	305.6	215.3
P	4	967	310.2	171.4	324	321.1	199.6
Q	5	929	289.2	222.4	250	294.4	234.9

Table 4.8: Species concentrations at the inlet and outlet of the reactor in mmol·L^{-1}. Species A—ethanol, B—water, C—hydrogen, D—carbon monoxide, E—methane, F—carbon dioxide, G—ethane

			Inlet (mmol·L^{-1})		Outlet (mmol·L^{-1})					
Run ID	DOE Line	T / K	C_{A0}	C_{B0}	C_B	C_C	C_D	C_E	C_F	C_G
A	13	983	95.9	3069.0	2722.8	206.7	6.0	71.1	86.8	3.5
B	8	967	115.1	3124.7	2720.5	234.3	6.9	88.0	99.4	7.9
C	11	944	98.3	3254.9	2898.6	199.8	3.7	74.9	86.8	7.8
D	3	930	206.5	3202.5	2589.6	337.9	16.2	154.8	151.8	20.1
E	7	930	137.7	3284.4	2837.6	247.8	7.4	101.1	109.4	13.1
F	12	901	106.8	3490.7	3065.1	230.3	2.6	80.5	98.1	7.2
G	10	944	98.8	3200.6	2840.7	199.7	2.6	78.1	88.7	8.5
H	17	941	57.6	3314.9	3070.7	133.4	1.6	45.4	56.5	5.3
I	1	931	70.4	3324.2	3054.3	149.4	1.3	55.4	60.9	5.8
J	2	967	79.7	3169.1	2864.8	188.3	1.5	54.4	69.6	5.1
K	15	943	213.2	3130.4	2515.8	343.4	13.0	163.7	155.4	21.5
L	6	964	52.0	3212.6	2990.7	130.5	0.1	40.9	48.3	3.6
M	16	944	169.6	3139.3	2635.1	285.5	7.3	133.2	124.5	13.8
N	14	944	19.1	3348.5	3251.7	52.8	0.0	13.3	20.0	1.4
O	9	944	100.5	3252.5	2904.2	198.1	2.8	74.5	84.9	8.3
P	4	967	191.9	3032.3	2466.5	326.4	12.9	150.6	144.8	13.0
Q	5	929	56.5	3401.9	3165.9	128.6	0.9	44.0	53.6	4.1

4.2 Mechanistic Elucidation of the Process

As shown in Table 4.2, the principal products of the supercritical water reformation of ethanol are hydrogen, carbon oxides, methane, and ethane. By examination of the product composition and atomic balances, as well as the selectivity of various products, the overall reaction schemes that take place in the supercritical water reformation of ethanol may be inferred.

4.2.1 Pyrolytic Decomposition of Ethanol and Water-gas Shift

The presence of methane in the effluent gas, in relatively high concentrations, between 15.1 and 23.5 mol-%, suggests that ethanol is being decomposed as

$$C_2H_5OH \rightarrow CH_4 + CO + H_2 \qquad (4.1)$$

The absence of acetaldehyde is significant since in published work at 773 K, acetaldehyde is an important intermediate in the decomposition of ethanol in supercritical water[14]:

$$C_2H_5OH \rightarrow CH_3CHO + H_2 \quad (4.2)$$

Acetaldehyde may be further decomposed to form methane and carbon monoxide:

$$CH_3CHO \rightarrow CH_4 + CO \quad (4.3)$$

The absence of acetaldehyde in the product mixture indicates that the decomposition of acetaldehyde to methane at the temperature ranges investigated went to completion or ethanol decomposes by other means such as direct single-stage decomposition. Regardless, the combination of (4.2) and (4.3) would yield (4.1):

$$C_2H_5OH \rightarrow CH_4 + CO + H_2 \quad (4.1)$$

Carbon monoxide appears in relatively low concentrations, between 0 and 2.4 mol-%. Carbon monoxide does not appear in equal molar quantities as methane, and there is an abundance of carbon dioxide in the product stream. Both are indicative of the mechanistic fact that the forward water-gas shift reaction is active at the conditions investigated:

$$CO + H_2O \rightarrow CO_2 + H_2 \quad (4.4)$$

By combining (4.1) and (4.4), the resultant stoichiometric equation, the pyrolytic decomposition of ethanol reaction, may be reduced to

$$C_2H_5OH + H_2O \rightarrow CH_4 + CO_2 + 2H_2 \quad (4.5)$$

Based on the stoichiometry of (4.5), if all ethanol molecules fed were converted predominantly by this reaction, then the molar ratios of CH_4/CO_2 and H_2/CO_2 would be

1:1 and 2:1, respectively. In addition, the molar ratio of H_2/CH_4 would be 2:1. Table 4.9 lists the molar ratios of various product gases.

As can be seen from the table, the ratios of H_2/CH_4 for all experimental runs range between 2.1 and 4.0, all exceeding 2.0, thus confirming that all of the hydrogen is not generated by this combinatory route between pyrolytic decomposition and water gas shift reactions. Rather, hydrogen generation has also been realized to a substantial extent via a more stoichiometrically favorable conversion route whose typical yield ratio of H_2/CH_4 is greater than 2.0. This is further elaborated in a later section.

Table 4.9 Ethanol to water ratio and product molar ratios

Run ID	DOE Line	T/K	$EtOH/H_2O$ (by mass)	$H_2O/EtOH$ (by mass)	$H_2/EtOH$	H_2/CO_X	H_2/CH_4	CH_4/CO_X	$CO_2/(CO+CO_2)$
A	13	983	8.0%	17.9	2.347	2.227	2.910	0.765	0.935
B	8	967	9.4%	15.2	2.255	2.204	2.664	0.827	0.935
C	11	944	7.7%	5.9	2.220	2.209	2.668	0.828	0.960
D	3	930	16.5%	6.0	1.918	2.011	2.184	0.921	0.903
E	7	930	10.7%	23.1	2.009	2.121	2.450	0.866	0.936
F	12	901	7.8%	23.6	2.373	2.288	2.862	0.799	0.974
G	10	944	7.9%	9.1	2.204	2.188	2.558	0.855	0.972
H	17	941	4.4%	10.4	2.458	2.297	2.937	0.782	0.972
I	1	931	5.4%	12.5	2.264	2.403	2.696	0.891	0.980
J	2	967	6.4%	12.4	2.562	2.647	3.463	0.764	0.979
K	15	943	17.4%	12.7	1.898	2.040	2.098	0.972	0.923
L	6	964	4.1%	12.4	2.650	2.696	3.187	0.846	0.997
M	16	944	13.8%	12.3	1.923	2.166	2.143	1.011	0.945
N	14	944	1.5%	67.6	2.861	2.640	3.963	0.666	1.000
O	9	944	7.9%	5.6	2.141	2.260	2.660	0.850	0.969
P	4	967	16.2%	7.0	1.982	2.070	2.168	0.955	0.918
Q	5	929	4.2%	21.9	2.397	2.361	2.921	0.808	0.984

The extent of the forward water-gas shift reaction is significant, being greater than 90% at all experimental conditions (Table 4.6). It is important to note that the water-gas shift reaction is a reversible reaction whose overall direction of reaction can be easily reversed by imposed conditions. At the temperatures at which the experiments were conducted, the water-gas shift reaction should be somewhat limited by chemical

equilibrium. A possible explanation for the high extent of the forward reaction is attributable to the fact that the high concentration of water is driving the water-gas shift reaction's equilibrium to favor the forward direction conversion. Another explanation is that there may be more than one phase in the reactor, a hydrogen-rich phase and a hydrogen-poor phase that contains mostly water and carbon-containing species. If hydrogen is not present in a phase where water and carbon monoxide are most abundantly present, the water-gas shift reaction would proceed in the forward direction without the full influence of an equilibrium limitation.

4.2.2 Direct Reformation Reaction of Ethanol

With hydrogen to methane ratios greater than 2, more hydrogen is being produced than the pyrolytic decomposition reaction would predict, which indicates that another hydrogen forming reaction is occurring outside of the decomposition reaction, and the forward water-gas shift reaction. The overall stoichiometric equation for the steam reformation of ethanol, or direct reformation of ethanol, is

$$C_2H_5OH + 3\ H_2O \rightarrow 2CO_2 + 6H_2 \qquad (4.6)$$

which may account for the additional hydrogen. If all the ethanol molecules fed were converted solely via this step (4.6), the molar ratios of CH_4/CO_2 and H_2/CO_2 would become 0:1 and 3:1, respectively.

At higher temperatures, methane can be further reacted via methane reformation and a subsequent water-gas shift reaction:

$$CH_4 + H_2O \rightarrow CO + 3H_2 \qquad (4.7)$$

$$CO + H_2O \rightarrow CO_2 + H_2 \qquad (4.4)$$

The resultant stoichiometric equation combining all three reactions, i.e., Eqns (4.4), (4.5), and (4.7), would become essentially the same as the direct reformation reaction of ethanol:

$$C_2H_5OH + 3\ H_2O \rightarrow 2CO_2 + 6H_2 \qquad (4.6)$$

As a result, a vital question regarding the mechanistic pathway for noncatalytic ethanol reformation in the supercritical water medium now becomes whether the reformation reaction proceeds via direct reformation, reaction (4.6), to produce hydrogen and carbon dioxide, or indirectly via methane reformation (4.4, 4.5, and 4.7) to produce hydrogen and carbon dioxide. Based on the preliminary study of JP-8 reformation kinetics[38], it was found that the reformation of methane at temperatures lower than 690°C is not appreciably significant. Thus, the methane reformation reaction was not heavily involved in most of the design point runs, except the ones for 710°C, listed in Table 4.6.

As can be clearly seen in Table 4.9, the molar ratios of CH_4/CO_2 and H_2/CO_2 for all experimental runs fall in the ranges of 0-1:1 and 2-3:1, respectively. This observation further indicates that the reactions represented by Eq. (4.5) and Eq. (4.6) are competitively taking place in the reaction system at the conditions investigated in the current study. However, it must be noted that the most efficient conversion scenario would involve maximizing the direct reformation reaction while minimizing the pyrolytic decomposition, with complete conversion of ethanol to gaseous product.

4.2.3 Dehydration of Ethanol

The presence of ethane suggests that there is an undesirable competing reaction, even though not a dominant one. Ethylene, a potential coking precursor, can be produced by

dehydration of ethanol. If there is a sufficient amount of product hydrogen present, ethylene can be hydrogenated *in situ* to form ethane by the following reactions:

dehydration: $C_2H_5OH \rightarrow C_2H_4 + H_2O$ (4.8)

hydrogenation: $C_2H_4 + H_2 \rightarrow C_2H_6$ (4.9)

Absence of acetylene in the product stream also indicates that the reaction environment favors hydrogenating rather than dehydrogenating ethylene. In addition, it is noteworthy that ethanol is still dehydrated via (4.8) in such a water-rich environment.

4.3 Kinetic Model

Since all of the reactant, ethanol, was consumed in the reformation reactions, the kinetic model is based on carbon balances, the conversion of ethanol to methane, and the conversion of ethanol to hydrogen. Global first-order kinetics is assumed for the pyrolytic decomposition of ethanol to methane:

$$C_2H_5OH + H_2O \xrightarrow{k_1} CH_4 + CO_2 + 2H_2 \quad (4.5)$$

with the rate of disappearance of ethanol for the decomposition reaction as

$$-\frac{dC_A}{dt} = k_1 C_A \quad (4.1)$$

For the direct reformation of ethanol into carbon dioxide, a multiplicative factor of the molar ratio of ethanol to water, Φ^n, is included in the global first-order rate expression:

$$C_2H_5OH + 3\ H_2O \xrightarrow{k_2} 2CO_2 + 6H_2 \quad (4.6)$$

with the rate of disappearance of ethanol for the reformation reaction

$$-\frac{dC_A}{dt} = k_2\ \Phi^n\ C_A \tag{4.2}$$

The inclusion of a multiplicative factor of Φ^n in the kinetic rate expression is to account for the ethanol-to-water feed ratio that is directly linked with the chemical equilibrium limitation imposed on the reformation reaction. Then, the overall rate expression for the disappearance of ethanol is

$$-\frac{dC_A}{dt} = k_1\ C_A + k_2\ \Phi^n\ C_A \tag{4.3}$$

which has the integrated rate expression:

$$C_A = C_{A0}\ \exp\left[-\left(k_1 + \Phi^n k_2\right)t\right] \tag{4.4}$$

The rates of generation of methane and hydrogen may be expressed as a function of the concentration of ethanol and are

$$\frac{dC_E}{dt} = k_1\ C_A \tag{4.5}$$

$$\frac{dC_C}{dt} = 2k_1\ C_A + 6\ k_2\ \Phi^n\ C_A \tag{4.6}$$

By substituting (4.4) into equations (4.5) and (4.6) and integrating, the expressions for the concentrations of hydrogen and methane are

$$C_C = C_{A0}\ \frac{2\ k_1 + 6\ \Phi^n\ k_2}{k_1 + \Phi^n\ k_2}\left(1 - \exp\left[-\left(k_1 + \Phi^n k_2\right)t\right]\right) \tag{4.7}$$

$$C_E = C_{A0}\ \frac{k_1}{k_1 + \Phi^n\ k_2}\left(1 - \exp\left[-\left(k_1 + \Phi^n k_2\right)t\right]\right) \tag{4.8}$$

where C_{A0} is the initial concentration of ethanol, k_1 and k_2 are first-order rate constants, and Φ^n is the molar feed ratio of ethanol to water. These equations can be solved simultaneously to find the rate constants k_1 and k_2 by setting C_{A0} as the inlet

concentration of ethanol in moles per liter, C_E is the outlet concentration of methane in moles per liter, and C_C is the outlet concentration of hydrogen. The concentration for each species is listed in Table 4.8.

The rate coefficients may then be regressed using a commercially available software package such as Maple 10. The calculated rate coefficients for the decomposition reaction and the reformation reaction are tabulated in Table 4.10.

Table 4.10: Calculated rate coefficients for the pyrolytic decomposition (1) and direct reformation (2) reactions

Run ID	DOE Line	$\Phi^{1.5}$	T^{-1}/K^{-1}	k_1	k_2
A	13	5.522E-03	1.017E-03	0.302477	0.045853
B	8	7.073E-03	1.035E-03	0.447696	0.049562
C	11	5.249E-03	1.059E-03	0.301882	0.033630
D	3	1.637E-02	1.075E-03	0.238523	0.007298
E	7	8.586E-03	1.075E-03	0.341979	0.025633
F	12	5.354E-03	1.109E-03	0.272997	0.039233
G	10	5.424E-03	1.059E-03	0.334345	0.031075
H	17	2.292E-03	1.062E-03	0.553869	0.086538
I	1	3.084E-03	1.074E-03	0.260636	0.030229
J	2	3.987E-03	1.035E-03	0.202829	0.049462
K	15	1.778E-02	1.060E-03	0.317803	0.005209
L	6	2.059E-03	1.037E-03	0.395480	0.078271
M	16	1.255E-02	1.059E-03	0.190206	0.004518
N	14	4.301E-04	1.060E-03	0.246838	0.080759
O	9	5.431E-03	1.060E-03	0.288272	0.031716
P	4	1.592E-02	1.035E-03	0.284378	0.007959
Q	5	2.138E-03	1.076E-03	0.363529	0.055794

The Arrhenius activation energy is defined by

$$k = A\, e^{-E_a/R\,T} \tag{4.9}$$

where k is the rate coefficient, A is the frequency factor, E_a is the activation energy, R is the gas law constant, and T is absolute temperature. The activation energy may be determined by linear regression of the natural logarithm of the rate coefficient versus the inverse of the temperature. The natural logarithm of the mean of the rate coefficient for

the pyrolytic decomposition reaction and the direct reformation reaction at the design of experiment's test temperatures are plotted in Figure 4.1.

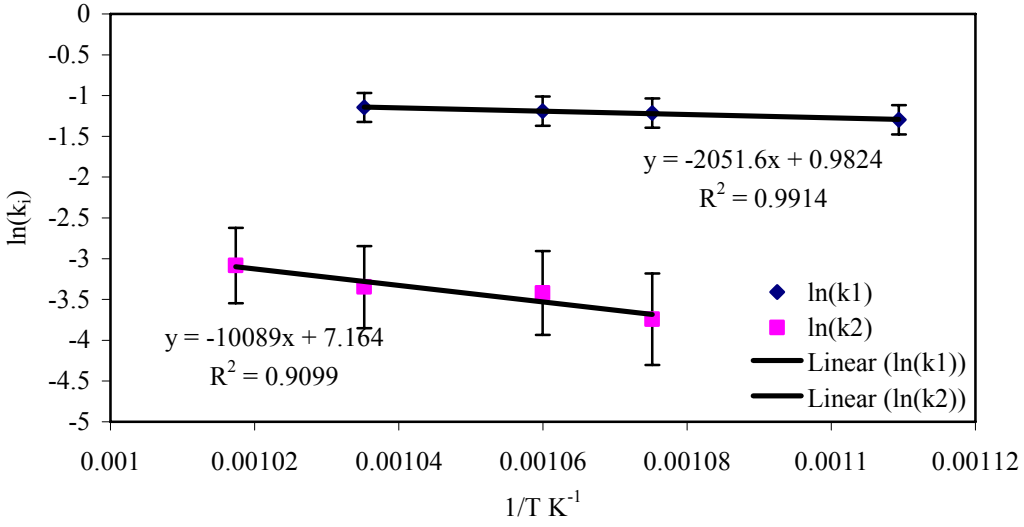

Figure 4.1: Arrhenius plot for the pyrolytic decomposition reaction (1) and the direct reformation reaction (2).

The rate constant k_1 refers to the pyrolytic decomposition reaction and k_2 refers to the direct reformation reaction. The error bars were determined from the standard error of the average logarithm of the rate constant at each temperature. For the pyrolytic reformation reaction, k_1, the greatest standard error was 0.18. For the direct reformation reaction, k_2, the standard error was 0.50. Based on the linear best fit of the Arrhenius plot, the Arrhenius activation energy and frequency factor values shown in Table 4.11 are obtained.

Table 4.11: Arrhenius activation energy.

	E_A (kJ/mol)	A	R^2
pyrolytic decomposition	17.1	2.67	0.99
direct reformation	83.9	1290	0.91

With a lower activation energy, the pyrolytic decomposition reaction is less temperature dependent than the direct reformation reaction. This remark is substantiated by previously published work[14], where the decomposition of ethanol combined with the water-gas shift reaction were the predominant reactions at 773 K. At this temperature, direct reformation was not reported. Due to the higher temperature dependence of the direct reformation reaction, this reaction will become more active at higher temperatures and will out-compete the decomposition reaction, thus maximizing the production of the desired product, hydrogen. It is also noteworthy that as temperatures increase above those tested, that the methane reformation reaction will contribute more to the product composition.

4.4 Optimization and Analysis of Variance

The three process conditions tested in this experimental design were temperature, ethanol feed rate, and water feed rate with a fixed pressure. There are several important parameters of mechanistic and kinetic interest that may be statically evaluated, which may provide further insight into improvements and optimization of supercritical water reformation of ethanol into hydrogen. Of particular interest is the conversion of ethanol into hydrogen, the selectivity of hydrogen over methane, and the selectivity of methane over carbon oxides.

4.4.1 Conversion of Ethanol into Hydrogen

The effectiveness of hydrogen generation, the goal of ethanol reformation, is evaluated by a statistical analysis of the molar ratio of hydrogen produced versus ethanol fed into

the reactor. An analysis of variance of the factorial portion of the design of experiments (DOE), Table 4.12, shows that only the main effects, temperature, ethanol flow rate, and water flow rate, are statically significant in terms of hydrogen production with $p \leq 0.05$. The interactive effects were not statistically significant. This may be due to the long residence times used for this design since the feed ethanol was completely converted as evidenced by practically no carbon content in the liquid phase of the reactor effluent. Table 4.13 shows the estimated effects and corresponding p-values.

Table 4.12 Analysis of variance for hydrogen generation.

Source	DF	Seq SS	Adj SS	Adj MS	F	P
Main Effects	3	0.503555	0.503555	0.167852	120.94	0.008
2-way Interactions	3	0.011041	0.011041	0.00368	2.65	0.286
3-way Interactions	1	0.00606	0.00606	0.00606	4.37	0.172
Curvature	1	0.009102	0.009102	0.009102	6.56	0.125
Residual Error	2	0.002776	0.002776	0.001388		
Pure Error	2	0.002776	0.002776	0.001388		
Total	10	0.532534				

Table 4.13 Estimated effects and test statistics for hydrogen generation.

Term	Effect	Coef	SE Coef	T	P
Constant		2.2552	0.01317	171.22	0
T	0.2106	0.1053	0.01317	7.99	0.015
F_{EtOH}	-0.4297	-0.2148	0.01317	-16.31	0.004
F_{H2O}	0.151	0.0755	0.01317	5.73	0.029
$T*F_{EtOH}$	-0.0573	-0.0286	0.01317	-2.17	0.162
$T*F_{H2O}$	0.0355	0.0177	0.01317	1.35	0.31
$F_{EtOH}*F_{H2O}$	0.0313	0.0157	0.01317	1.19	0.356
$T*F_{ETOH}*F_{H2O}$	0.055	0.0275	0.01317	2.09	0.172
Ct Pt		-0.0646	0.02522	-2.56	0.125

Contour plots of the response surface for hydrogen to ethanol molar ratios were generated using Minitab® statistical software and are shown in Figure 4.2. Since the interactive effects are not statistically significant, conclusions cannot be drawn with statistical certainty using the contour plots. However, some trends may be inferred:

hydrogen production is highest at higher temperatures, at higher water flow rates, and at the lower ethanol flow rates tested.

The flow rates of water and ethanol affect both residence time and ethanol feed concentrations (ethanol to water ratio). Since more hydrogen appears to be produced at the lowest ethanol flow rates, it is apparent that lower ethanol to water ratios allow for more hydrogen to be produced. This is also consistent with the fact that the lowest ethanol-to-water feed ratio generates the highest molar ratio of hydrogen to methane in the product stream, thus maximizing the reformation efficiency. Please refer to Run N in Table 4.6.

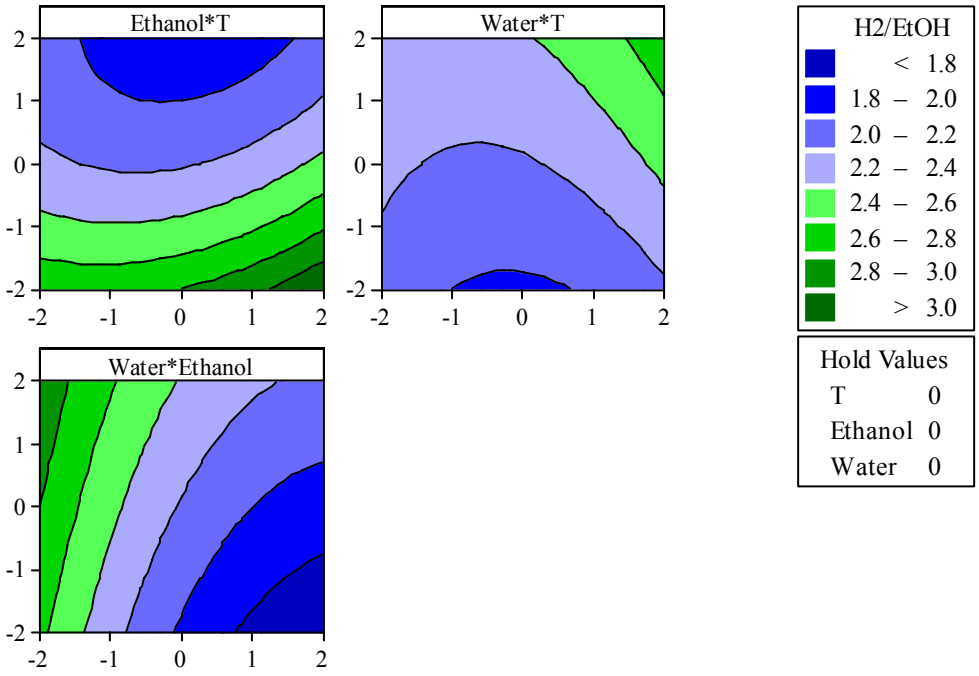

Figure 4.2: Contour plots of DOE for hydrogen to ethanol molar ratio, clockwise starting with the top left contour plot: (1) ethanol flow rate versus temperature with water flow held constant, (2) water flow rate versus temperature, ethanol flow held constant, (3) water flow rate versus ethanol flow rate, temperature held constant.

4.4.2 Selectivity of Hydrogen over Methane

The selectivity of hydrogen over methane is important in evaluating the competitive nature between the direct reformation reaction and the pyrolytic decomposition reaction. The direct reformation reaction is desirable over the pyrolytic decomposition reaction since, when combined with the forward water gas shift reaction, produces three times more hydrogen than the pyrolytic decomposition reaction. In addition, if the pyrolytic decomposition reaction were the sole or dominant reaction, the hydrogen to methane ratio would be 2:1. At conditions where this ratio increases, the direct reformation reaction is more active. Table 4.14 is the analysis of variance of the factorial portion of the DOE for the selectivity of hydrogen over methane.

Table 4.14 Analysis of variance for hydrogen selectivity over methane.

Source	DF	Seq SS	Adj SS	Adj MS	F	P
Main Effects	3	1.2333	1.2333	0.4111	109.30	0.009
2-way Interactions	3	0.1790	0.1790	0.0597	15.86	0.060
3-way Interactions	1	0.0668	0.0668	0.0668	17.76	0.052
Curvature	1	0.0169	0.0169	0.0169	4.49	0.168
Residual Error	2	0.0075	0.0075	0.0038		
Pure Error	2	0.0075	0.0075	0.0038		
Total	10	1.503				

As shown in Table 4.14, the main effects, temperature, ethanol flow rate, and water flow rate, are statically significant in terms of hydrogen selectivity over methane with $p \leq 0.05$. The two and three way interactions are statically significant with $p \leq 0.10$. Table 4.15 shows the estimated effects and corresponding p-values.

The contour plots of the response surface of the selectivity of hydrogen over methane are shown in Figure 4.3. The contour plot of the selectivity with ethanol flow rate versus temperature with the water flow rate held constant, plot (1), shows that with increasing temperature, a greater amount of hydrogen is produced in relation to methane.

In addition, the more ethanol that is feed, hence decreasing water to ethanol ratio, the selectivity of hydrogen over methane decreases regardless of the temperature. In comparing contour plots (2) and (3), it is evident that as the ethanol amount in water increases, the selectivity of hydrogen over methane decreases. As a result, over the range of conditions tested, the selectivity of hydrogen over methane is highly dependent up the water to ethanol ratio.

Table 4.15 Estimated effects and test statistics for hydrogen selectivity over methane.

Term	Effect	Coef	SE Coef	T	P
Constant		2.7166	0.02168	125.29	0
T	0.3077	0.1539	0.02168	7.1	0.019
F_{EtOH}	-0.7002	-0.3501	0.02168	-16.15	0.004
F_{H2O}	0.1777	0.0889	0.02168	4.1	0.055
$T*F_{EtOH}$	-0.2087	-0.1044	0.02168	-4.81	0.041
$T*F_{H2O}$	-0.0677	-0.0339	0.02168	-1.56	0.259
$F_{EtOH}*F_{H2O}$	0.2033	0.1016	0.02168	4.69	0.043
$T*F_{ETOH}*F_{H2O}$	0.1828	0.0914	0.02168	4.21	0.052
Ct Pt		-0.088	0.04152	-2.12	0.168

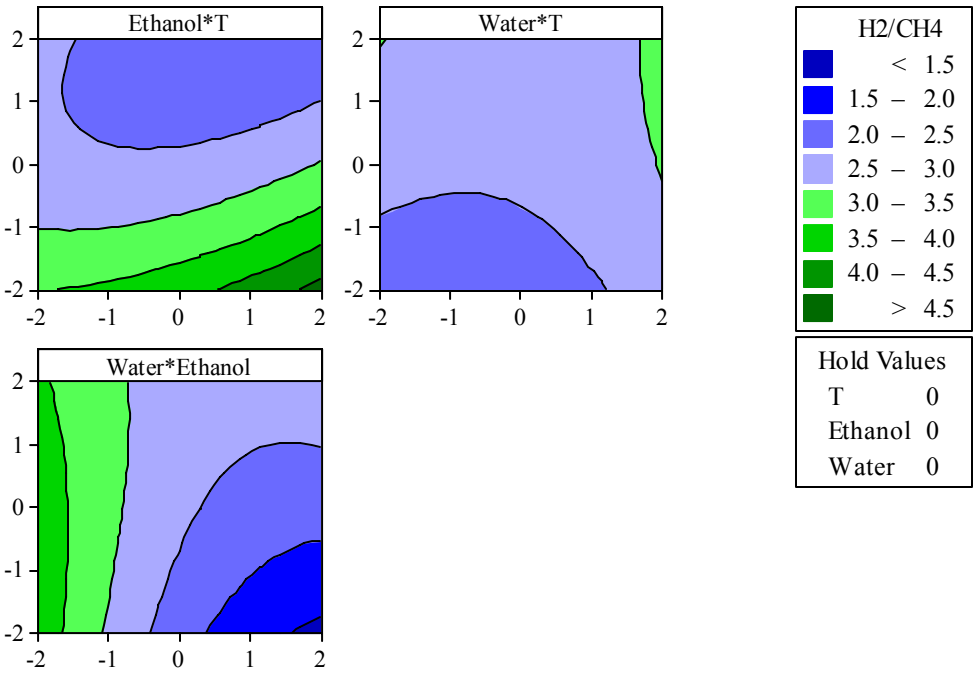

Figure 4.3: Contour plots of DOE for hydrogen over methane selectivity, clockwise starting with the top left contour plot: (1) ethanol flow rate versus temperature with water flow held constant, (2) water flow rate versus temperature, ethanol flow held constant, (3) water flow rate versus ethanol flow rate, temperature held constant.

4.5 Comparisons between Experiments

Comparisons between experiments where only one or two conditions are varied and the reminder are held constant provides further insight into the kinetic relationships of supercritical water reforming of ethanol into hydrogen, which can be used to determine optimal operating conditions.

4.5.1 Comparisons between Water to Ethanol Ratios

For this work, the water feed rate, ethanol feed rate, and temperature were varied. As a result there are several experiments where the ratio of the water fed over the ethanol fed changed, but the temperature and the space time remained constant. By comparing experiments with constant temperature and space times the effects of varying the water to

ethanol ratios upon hydrogen selectivity, hydrogen concentration, and ethanol conversion are determined.

For experiments Q and E, the temperature was 930 K, the space time was 240±10 s, and the respective water to ethanol ratios were 23.1 and 9.1. The respective hydrogen selectivity over methane was 2.9 and 2.5. In addition, the ratio of carbon dioxide to carbon oxides was 0.98 and 0.94 respectively. This indicates that higher water to ethanol ratios enhances the hydrogen selectivity over methane and the forward water-gas shift reaction. A similar comparison may be drawn for experiments D and I where the temperature was 930 K, the space time was 352±4 s, and the respective water to ethanol ratios were 5.9 and 17.9. The hydrogen selectivity over methane was 2.2 and 2.7.

Likewise for experiments N and G, the temperature was 944 K, the space time was 285±5 s, and the respective water to ethanol ratios were 67.6 and 12.4. The respective hydrogen selectivity over methane was 4.0 and 2.6 and the ratio of carbon dioxide to carbon oxides was 1.00 and 0.97. This also indicates that higher water to ethanol ratios enhances hydrogen selectivity over methane and the forward water-gas shift reaction.

As shown in Figure 4.4, as the water to ethanol ratio increases, the selectivity of hydrogen over methane increases, meaning that the direct reformation reaction becomes preferred over the pyrolytic decomposition reaction. The selectivity increases linearly for experimental conditions between 930 K and 944 K, and space times between 233 and 356 seconds, and for water to ethanol ratios between 5.6 and 23. Experiment N had the greatest water to ethanol ratio of all experiments conducted of 67.1. As seen on Figure 4.4, the selectivity of hydrogen over methane is lower than the linear trend would predict.

The lower than expected selectivity for hydrogen over methane in Experiment N may be caused by an equilibrium limitation in regards to the direct reformation reaction in respect to ethanol concentration.

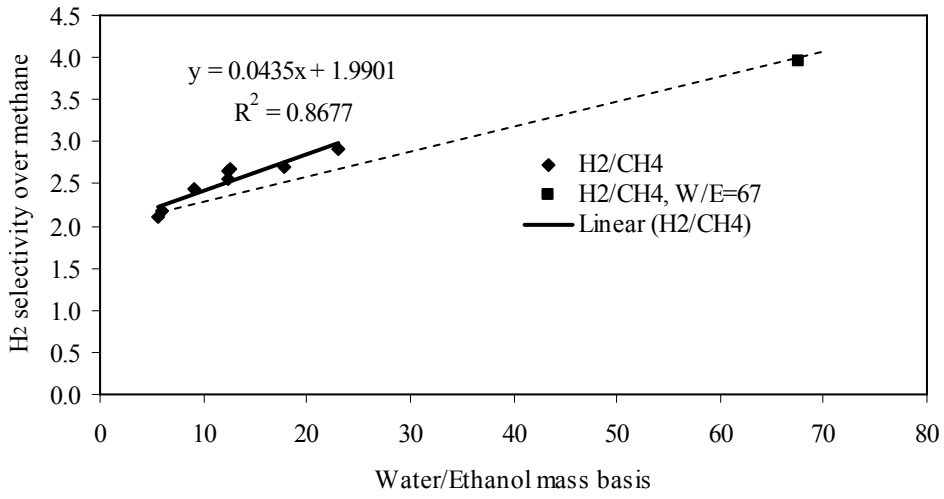

Figure 4.4: Hydrogen selectivity over methane versus water to ethanol feed ratio for runs between 930 and 944 K and space times between 233 and 356 s, solid line linear regression, dashed line connects minimum and maximum water to ethanol ratio points.

4.5.2 Comparisons between Temperatures

For experiments D and P, the water to ethanol ratio was 6, the space time was 336±12 s, and the reaction temperatures were respectively 930 K and 967 K. The respective selectivity of hydrogen over methane was nearly the same at 2.18 and 2.17. The ratios of hydrogen produced to ethanol fed, which is indicative of the extent of the reformation reactions, were 1.92 and 1.98 respectively, which is similar. Considering the substantial temperature difference between the two experiments, the hydrogen selectivity is quite remarkable. This result may indicate that the reaction may have reached an equilibrium-limited point at the temperatures for experiments D and P.

Experiment K has nominally similar reaction conditions to experiments D and P with the exception of a space time of 275 s (shorter by 59 s) and a temperature of 943 K. The selectivity of hydrogen over methane was 2.10 and the ratio of hydrogen produced to ethanol fed was 1.90. It can be readily noted that the extents of the reactions producing hydrogen in experiments D and P are higher than experiment K. Likewise the selectivity of hydrogen over methane is slightly lower in experiment K. Since a shorter reaction time coupled with a higher reaction temperature was employed for experiment K under otherwise nominally similar conditions as experiment D, the ratio of hydrogen produced to ethanol fed and the selectivity of hydrogen over methane should not be higher in D when compared to K, unless the reactions are limited by equilibrium, or are past the equilibrium conversion.

In comparing experiments C and F, where the water to ethanol ratio was approximately 12.5 and the space time was 296±11 s, the only difference in the reaction conditions was the temperature, respectively 901 K and 944 K. The resultant hydrogen over methane selectivity was 2.86 and 2.67 and the resultant hydrogen produced over ethanol fed was 2.4 and 2.2 respectively at the conditions investigated. Considering the large difference in temperature, 43 K, between the two cases, the conversion difference is relatively minor, which indicates that the temperature and space time conditions considered encompasses the maximum conversion in the region, which is very similar to the conclusion for experiments D and P.

The same conclusion can be drawn between experiments F and A, the minimum and maximum temperatures investigated. For experiment A, the ethanol ratio was 12.3, the space time was 268 s, and the temperature was 983. The ratio of hydrogen produced

over ethanol fed was 2.3 and selectivity of hydrogen over methane was 2.91. The temperature difference between F and A was 82 K, though the selectivity of hydrogen over methane and the ratio of hydrogen produced over ethanol fed were approximately the same. This indicates at the space time and feed conditions considered for these two experiments that the reactions had reached their maximum conversion for the temperatures considered.

For experiment O, the temperature was 944 K, the water to ethanol ratio was 12.5, and the space time was 281. In comparing experiment A and O, the major difference was the temperature, 983 K versus 944 K. The hydrogen selectivity over methane for experiment O was 2.66. Considering the large temperature difference, the difference in selectivity is rather small. This result also strongly indicates that the higher temperature experiment, A, has already reached or past the maximum equilibrium conversion.

In comparing experiments A, C, F, G, and O altogether, the space time and water to ethanol fed ratio may all be considered about equal. The resultant hydrogen concentration, 0.20-0.23 mol $\cdot L^{-1}$, and methane concentrations, 0.071-0.080 mol $\cdot L^{-1}$, were nearly unaffected by the change in temperature. This also indicates that the most important parameter for determining the hydrogen conversion and hydrogen selectivity of the process is the water-to-ethanol ratio.

4.5.3 Comparisons between Space Times

For experiment K the water to ethanol ratio was 5.6 and the space time was 275 s. For experiment M the water to ethanol ratio was 7.0 and the space was 486 s. For both experiments, the temperature was approximately 943 K, with the only difference being the space time. The selectivity of hydrogen over methane was nearly the same at 2.10

and 2.14, receptively, and the ratio of hydrogen produced over ethanol fed for both experiments was approximately 1.9. Thus at the conditions considered, the reactions have reached their maximum conversion for the residence times considered. The significance of this result is that a greater throughput for the existing reactor can be achieved without affecting conversion.

CHAPTER 5

CONCLUSIONS

Ethanol, a renewable resource, may be reformed into hydrogen non-catalytically using supercritical water, which acts synergistically both as a solvent and as a reactant. Supercritical water acts as a non-polar solvent which is completely miscible with ethanol and can form a binary supercritical mixture with ethanol at any concentration. Supercritical water reformation of ethanol avoids many of the typical pitfalls of catalytic steam reformation, including coke formation, fouling, sintering, poisoning, and deactivation. As a result, supercritical water reformation is a versatile and robust means of reforming ethanol and does not require pretreatment or refinement of the ethanol feedstock.

Supercritical water reformation of ethanol at the conditions tested occurs by two principal reactions: direct reformation of ethanol to hydrogen and carbon oxides, and pyrolytic decomposition of ethanol to hydrogen, methane, and carbon oxides. In this system the forward water-gas shift reaction is active even without the presence of a water gas shift catalyst. An undesirable, competing reaction occurs to some extent: dehydration of ethanol to form ethylene. Ethylene is subsequently hydrogenated to form ethane. This reaction not only consumes a desired product, hydrogen, but also produces a potential coking precursor, ethylene. However, upon inspection of the reactor, no coking was evidenced under the process conditions investigated in this study.

The pyrolytic reformation reaction modeled using global first order kinetics is found to have a regressed Arrhenius activation energy of 17.1 kJ/mol. The direct reformation reaction based on pseudo-first-order kinetics is found to have a regressed

Arrhenius activation energy of 83.9 kJ/mol. Comparing the two principal reaction mechanistic steps, the direct reformation reaction is found to be far more sensitive to the reaction temperature than the pyrolytic decomposition reaction.

This study introduces a new process synthesis route for generating hydrogen using a renewable agricultural feedstock of ethanol and elucidates pertinent chemical reaction mechanisms involved in the novel supercritical reformation process system. This study is the first of its kind to elucidate that the ethanol reformation using supercritical water takes place competitively between the pyrolytic decomposition of ethanol and the direct reformation of ethanol, both of which contribute to hydrogen production. The current study further establishes that water-gas shift reaction goes to near completion in the supercritical water medium under the conditions investigated, thus eliminating a separate gas-enriching step or a post-treatment stage through a catalyst bed. The current study also establishes that ethanol in a supercritical water medium is subjected to alcohol dehydration generating ethylene and the reaction environment involving ethylene is more hydrogenating rather than dehydrogenating.

Future experimental studies need to be performed to elucidate the effects of the changing nature of the fluid phase behavior along the reactor length upon the reaction kinetics, which will provide for an optimal reactor design and scale-up. Further, embedding the methane reformation reaction in the process scheme would enhance the ultimate conversion and resultant efficacy of the reformation process.

Table A.1: Composition of GC calibration gases.

Name	Manufacturer	Catalog Number	H_2 / mol-%	N_2 / mol-%	O_2 / mol-%	CO / mol-%	CH_4 / mol-%	CO_2 / mol-%	C_2H_2 / mol-%	C_2H_4 / mol-%	C_2H_6 / mol-%
Hydrogen	Airgas	HY 200	99%								
Nitrogen	Airgas	NI 200		99%							
Oxygen	Airgas	OX 200			99%						
Carbon Monoxide	Airgas	CM CP300				99.5%					
Methane	Airgas	ME CP200					99%				
Carbon Dixoide	Airgas	CD I200						99.99%			
Mix 7			40%	23%	6%			30%			
Mix 8			14%	19%	5%			63%			
Silver	Supelco	23462		#######		1.000%	0.999%	1.00%	1.000%	1.000%	1.020%
Blue	Supelco	501743		69.54%	4.00%	6.99%	4.50%	14.97%			

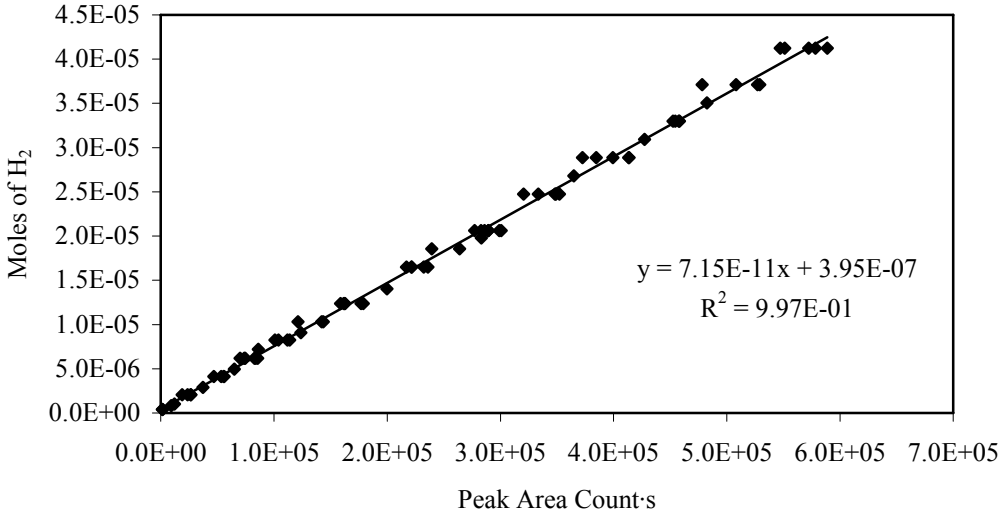

Figure A.1: GC calibration curve for hydrogen.

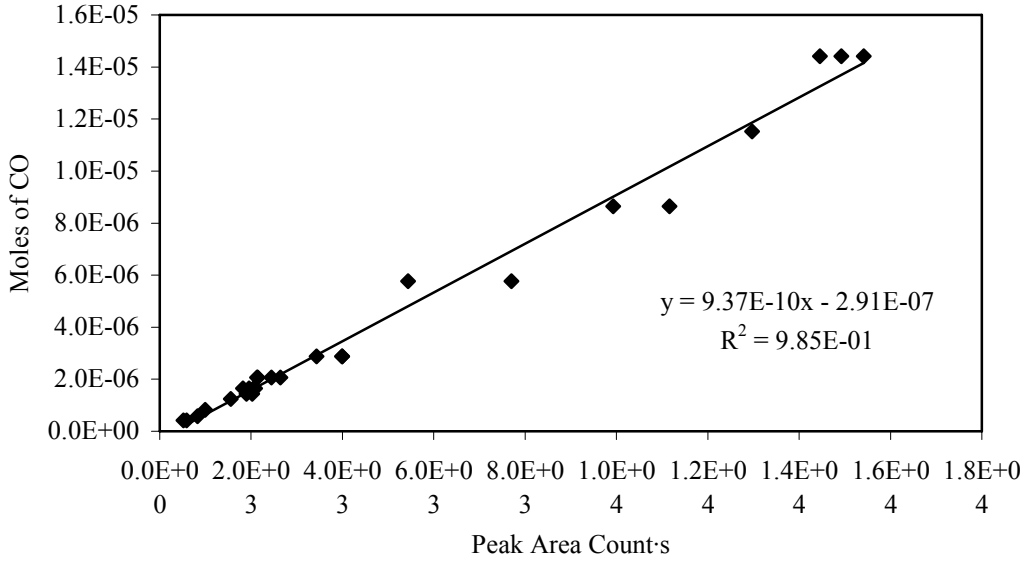

Figure A.2: GC calibration curve for carbon monoxide.

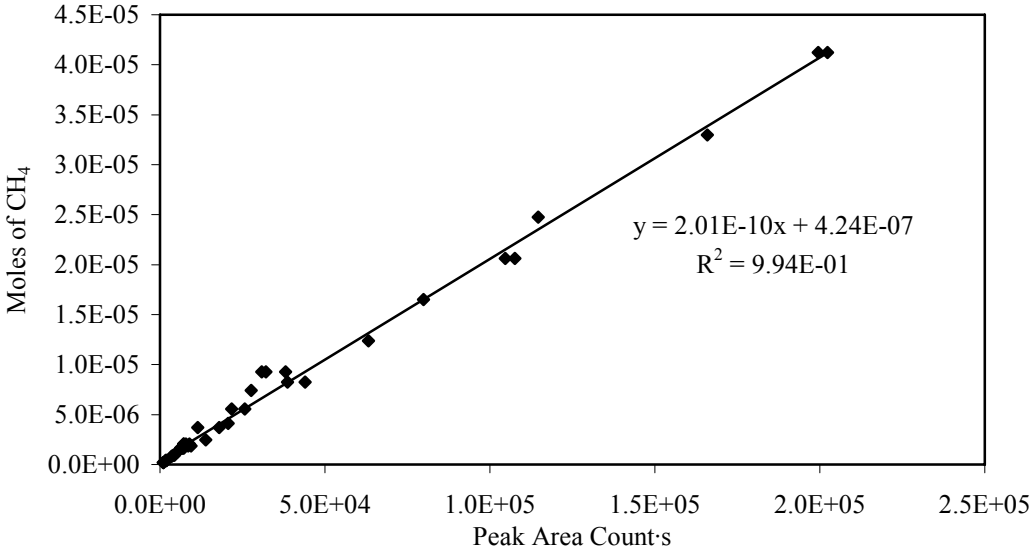

Figure A.3: GC calibration curve for methane.

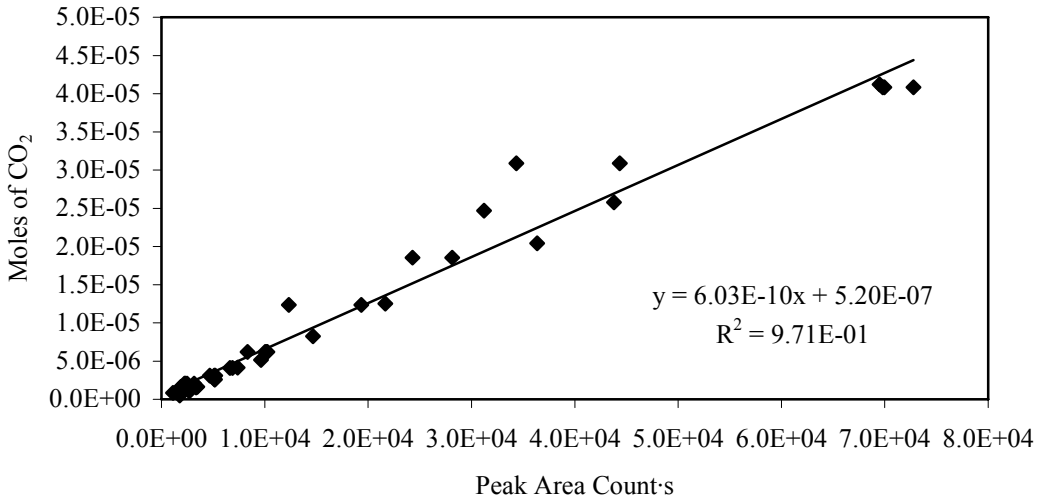

Figure A.4: GC calibration curve for carbon dioxide.

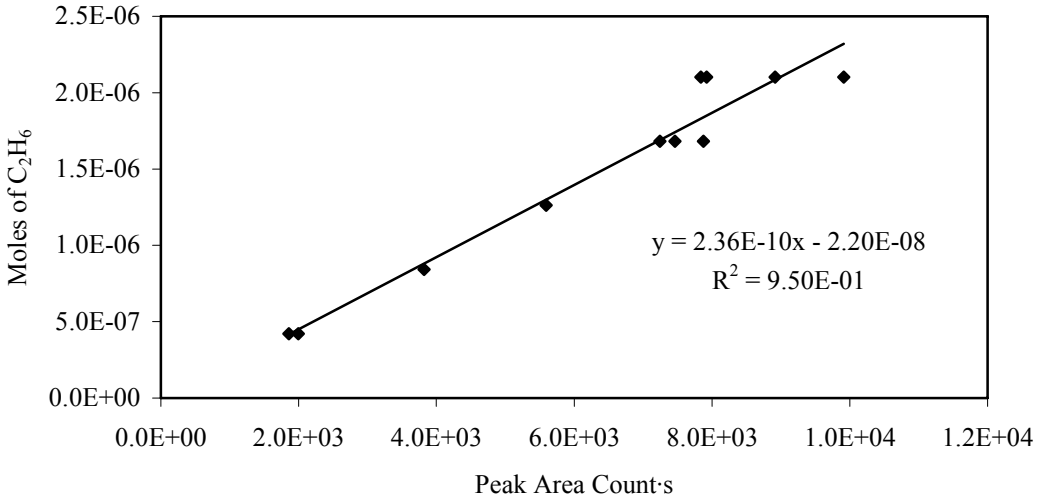

Figure A.5: GC calibration curve for ethane.

Table A.2 GC Calibration data for hydrogen.

Inj. Vol/ mL	Signal File	Area Count·s	H_2 / mol	Inj. Vol/ mL	Signal File	Area Count·s	H_2 / mol
0.50	Sig21483	300624.8	2.062E-05	0.40	Sig21708	232259.8	1.649E-05
0.50	Sig21485	299120.5	2.062E-05	0.90	Sig21709	527034.4	3.711E-05
0.10	Sig21487	53434.3	4.123E-06	0.50	Sig21710	289443.1	2.062E-05
0.70	Sig21488	413437.5	2.886E-05	0.75	Sig21711	427329.6	3.092E-05
0.40	Sig21489	235894.8	1.649E-05	0.65	Sig21712	364937.3	2.680E-05
0.70	Sig21490	413346.3	2.886E-05	0.80	Sig21713	454383.6	3.299E-05
0.15	Sig21491	74537.9	6.185E-06	0.50	Sig21714	282774.1	2.062E-05
0.60	Sig21493	352187.9	2.474E-05	0.85	Sig21715	482371.3	3.505E-05
0.05	Sig21494	23779.0	2.062E-06	0.15	Sig21716	85722.9	6.185E-06
0.10	Sig21495	46991.3	4.123E-06	0.90	Sig21717	508028.1	3.711E-05
0.60	Sig21496	320358.9	2.474E-05	1.00	Sig21718	550991.2	4.123E-05
0.40	Sig21997	217030.4	1.649E-05	0.50	Sig21719	286092.1	2.062E-05
0.20	Sig21498	100816.8	8.246E-06	0.80	Sig21720	452492.7	3.299E-05
0.90	Sig21499	478123.2	3.711E-05	1.00	Sig21722	578243.3	4.123E-05
0.18	Sig21501	86111.2	7.216E-06	0.30	Sig21723	176990.0	1.237E-05
0.45	Sig21502	239435.4	1.855E-05	0.05	Sig21724	26701.7	2.062E-06
0.30	Sig21503	158851.7	1.237E-05	0.25	Sig21725	143573.4	1.031E-05
0.15	Sig21505	70058.9	6.185E-06	0.10	Sig21726	55746.9	4.123E-06
0.70	Sig21506	372451.0	2.886E-05	0.01	Sig21727	1487.6	4.123E-07
0.40	Sig21556	221691.4	1.649E-05	0.20	Sig21728	113806.1	8.246E-06
0.30	Sig21557	162770.8	1.237E-05	0.50	Sig21729	289367.9	2.062E-05
0.70	Sig21558	384685.7	2.886E-05	0.10	Sig21730	55852.2	4.123E-06
1.00	Sig21559	547236.1	4.123E-05	0.02	Sig21731	9210.8	8.246E-07
0.15	Sig25160	73788.2	6.185E-06	0.15	Sig21732	82719.6	6.185E-06
0.40	Sig21561	221657.1	1.649E-05	0.03	Sig21733	12212.8	1.031E-06
0.20	Sig21562	104042.3	8.246E-06	0.45	Sig21734	263962.2	1.855E-05
0.60	Sig21563	333388.1	2.474E-05	0.05	Sig21735	26460.3	2.062E-06
0.50	Sig21564	277345.4	2.062E-05	0.01	Sig21736	1667.7	4.123E-07
0.30	Sig21565	161769.6	1.237E-05	0.15	Sig21737	83915.0	6.185E-06
0.05	Sig21566	19029.7	2.062E-06	0.25	Sig21738	142127.0	1.031E-05
0.30	Sig21567	162306.9	1.237E-05	0.34	Sig21739	199677.9	1.402E-05
0.25	Sig21569	121376.4	1.031E-05	0.48	Sig21740	283184.6	1.979E-05
1.00	Sig21701	588546.1	4.123E-05	0.60	Sig21741	348288.2	2.474E-05
0.90	Sig21702	529072.6	3.711E-05	0.30	Sig21743	178803.6	1.237E-05
0.80	Sig21703	458151.7	3.299E-05	0.22	Sig21744	123730.9	9.071E-06
0.80	Sig21704	457498.5	3.299E-05	0.12	Sig21745	65093.8	4.948E-06
0.70	Sig21705	399370.5	2.886E-05	0.07	Sig21746	37420.4	2.886E-06
1.00	Sig21706	572350.3	4.123E-05	0.20	Sig21747	111847.7	8.246E-06
0.60	Sig21707	348973.3	2.474E-05				

Table A.3: GC calibration data for carbon monoxide.

Source	Inj. Vol/ mL	mol-frac	Signal File	Area Count·s	CO / mol
Supelco 501743	0.2	0.0699	Sig20397	823.3	5.764E-07
Supelco 501743	0.5	0.0699	Sig20396	2025.4	1.441E-06
Supelco 501743	0.5	0.0699	Sig20411	1901.5	1.441E-06
Supelco 23462	1.0	0.0100	Sig20282	585.6	4.123E-07
Supelco 23462	1.0	0.0100	Sig20442	516.4	4.123E-07
Supelco 501743	1.0	0.0699	Sig20392	3993.0	2.882E-06
Supelco 501743	1.0	0.0699	Sig20398	3992.5	2.882E-06
Supelco 501743	1.0	0.0699	Sig20425	3435.9	2.882E-06
Supelco 23462	2.0	0.0100	Sig20422	995.1	8.246E-07
Supelco 501743	2.0	0.0699	Sig20395	7699.6	5.764E-06
Supelco 501743	2.0	0.0699	Sig20443	5438.0	5.764E-06
Supelco 23462	3.0	0.0100	Sig20416	1558.7	1.237E-06
Supelco 501743	3.0	0.0699	Sig20393	11158.8	8.646E-06
Supelco 501743	3.0	0.0699	Sig20413	9930.0	8.646E-06
Supelco 23462	4.0	0.0100	Sig20424	2089.9	1.649E-06
Supelco 23462	4.0	0.0100	Sig20441	1822.9	1.649E-06
Supelco 23462	4.0	0.0100	Sig20488	1955.4	1.649E-06
Supelco 23462	4.0	0.0100	Sig20489	2054.2	1.649E-06
Supelco 501743	4.0	0.0699	Sig20421	12970.9	1.153E-05
Supelco 23462	5.0	0.0100	Sig20415	2140.8	2.062E-06
Supelco 23462	5.0	0.0100	Sig20439	2638.8	2.062E-06
Supelco 23462	5.0	0.0100	Sig20444	2131.7	2.062E-06
Supelco 23462	5.0	0.0100	Sig20490	2442.0	2.062E-06
Supelco 501743	5.0	0.0699	Sig20412	15413.6	1.441E-05
Supelco 501743	5.0	0.0699	Sig20423	14922.9	1.441E-05
Supelco 501743	5.0	0.0699	Sig20440	14452.9	1.441E-05

Table A.4: GC calibration data for methane.

Source	Inj. Vol/ mL	mol-frac	Signal File	Area Count·s	CH_4 / mol
Methane 2.0	0.06	0.99	Sig20785	13927.8	2.474E-06
Methane 2.0	0.10	0.99	Sig20784	20698.1	4.123E-06
Methane 2.0	0.20	0.99	Sig20776	38663.9	8.246E-06
Methane 2.0	0.20	0.99	Sig20782	43976.8	8.246E-06
Methane 2.0	0.30	0.99	Sig20779	63194.3	1.237E-05
Methane 2.0	0.40	0.99	Sig20783	79915.4	1.649E-05
Methane 2.0	0.50	0.99	Sig20781	104671.0	2.062E-05
Methane 2.0	0.50	0.99	Sig20772	107570.0	2.062E-05
Methane 2.0	0.60	0.99	Sig20780	114700.0	2.474E-05
Methane 2.0	0.80	0.99	Sig20778	165943.0	3.299E-05
Methane 2.0	1.00	0.99	Sig20775	199526.0	4.123E-05
Methane 2.0	1.00	0.99	Sig20771	202311.0	4.123E-05
Supelco 23462	0.50	0.0099	Sig20418	982.1	2.062E-07
Supelco 23462	0.50	0.0099	Sig20417	1068.0	2.062E-07
Supelco 23462	1.00	0.0099	Sig20442	1729.0	4.082E-07
Supelco 23462	1.00	0.0099	Sig20282	1907.9	4.082E-07
Supelco 23462	2.00	0.0099	Sig20422	3617.4	8.164E-07
Supelco 23462	3.00	0.0099	Sig20416	5158.9	1.225E-06
Supelco 23462	4.00	0.0099	Sig20441	6166.8	1.633E-06
Supelco 23462	4.00	0.0099	Sig20488	6505.3	1.633E-06
Supelco 23462	4.00	0.0099	Sig20489	6826.4	1.633E-06
Supelco 23462	5.00	0.0099	Sig20444	7185.0	2.041E-06
Supelco 23462	4.00	0.0099	Sig20424	7197.2	1.633E-06
Supelco 23462	5.00	0.0099	Sig20415	7223.0	2.041E-06
Supelco 23462	5.00	0.0099	Sig20490	7895.8	2.041E-06
Supelco 23462	5.00	0.0099	Sig20439	8954.3	2.041E-06
Supelco 501743	0.20	0.0450	Sig20397	1930.8	3.711E-07
Supelco 501743	0.50	0.0450	Sig20411	4081.2	9.277E-07
Supelco 501743	0.50	0.0450	Sig20396	4400.8	9.277E-07
Supelco 501743	1.00	0.0450	Sig20425	7445.1	1.855E-06
Supelco 501743	1.00	0.0450	Sig20398	8589.5	1.855E-06
Supelco 501743	1.00	0.0450	Sig20392	9390.6	1.855E-06
Supelco 501743	2.00	0.0450	Sig20443	11499.6	3.711E-06
Supelco 501743	2.00	0.0450	Sig20395	18009.0	3.711E-06
Supelco 501743	3.00	0.0450	Sig20413	21712.5	5.566E-06
Supelco 501743	3.00	0.0450	Sig20393	25724.3	5.566E-06
Supelco 501743	4.00	0.0450	Sig20421	27650.7	7.422E-06
Supelco 501743	5.00	0.0450	Sig20440	30921.0	9.277E-06
Supelco 501743	5.00	0.0450	Sig20423	32135.1	9.277E-06
Supelco 501743	5.00	0.0450	Sig20412	38093.8	9.277E-06

Table A.5: GC calibration data for carbon dioxide.

Source	Inj. Vol/ mL	mol-frac	Signal File	Area Count·s	CO_2 / mol
CO2 4.0	1.00	0.9999	Sig20030	72777.8	4.0820E-05
CO2 4.0	1.00	0.9999	Sig20031	69958.9	4.0820E-05
CO2 4.0	0.10	0.9999	Sig20032	6873.3	4.0820E-06
CO2 4.0	0.10	0.9999	Sig20033	6646.3	4.0820E-06
CO2 4.0	1.00	0.9999	Sig20034	69815.7	4.0820E-05
CO2 4.0	0.50	0.9999	Sig20037	36362.1	2.0410E-05
Mix 7	1.00	0.303	Sig20069	21650.6	1.2493E-05
Mix 7	0.10	0.303	Sig20070	2225.6	1.2493E-06
Mix 8	1.00	0.625	Sig20224	43801.5	2.5770E-05
Mix 8	0.10	0.625	Sig20225	5139.4	2.5770E-06
Mix 8	0.02	0.625	Sig20226	1753.2	5.1540E-07
Mix 8	0.20	0.625	Sig20230	9638.3	5.1540E-06
Mix 8	0.06	0.625	Sig20232	3346.3	1.5462E-06
Mix 8	0.04	0.625	Sig20233	2710.1	1.0308E-06
Mix 8	0.10	0.625	Sig20234	5167.6	2.5770E-06
Supelco 501743	1.00	0.1497	Sig20392	10168.9	6.1725E-06
Supelco 501743	3.00	0.1497	Sig20393	28148.6	1.8517E-05
Supelco 501743	2.00	0.1497	Sig20395	19333.4	1.2345E-05
Supelco 501743	0.50	0.1497	Sig20396	5118.6	3.0862E-06
Supelco 501743	0.20	0.1497	Sig20397	2160.7	1.2345E-06
Supelco 501743	1.00	0.1497	Sig20398	10037.7	6.1725E-06
Supelco 501743	0.50	0.1497	Sig20411	4684.8	3.0862E-06
Supelco 501743	3.00	0.1497	Sig20413	24301.2	1.8517E-05
Supelco 501743	4.00	0.1497	Sig20421	31201.7	2.4690E-05
Supelco 23462	5.00	0.0100	Sig20415	2489.2	2.0616E-06
Supelco 23462	3.00	0.0100	Sig20416	1831.1	1.2370E-06
Supelco 23462	2.00	0.0100	Sig20395	1129.5	8.2465E-07
Supelco 501743	5.00	0.1497	Sig20423	44346.7	3.0862E-05
Supelco 23462	4.00	0.0100	Sig20424	2378.0	1.6493E-06
Supelco 501743	1.00	0.1497	Sig20425	8335.8	6.1725E-06
Supelco 23462	5.00	0.0100	Sig20439	3147.8	2.0616E-06
Supelco 501743	5.00	0.1497	Sig20440	34345.5	3.0862E-05
Supelco 501743	2.00	0.1497	Sig20443	12350.2	1.2345E-05
Supelco 501743	1.00	0.1497	Sig20961	10255.3	6.1725E-06
Supelco 501743	0.50	0.1497	Sig20962	5217.9	3.0862E-06
Supelco 23462	4.00	0.0100	Sig20441	1995.3	1.6493E-06
Supelco 23462	5.00	0.0100	Sig20444	2235.7	2.0616E-06
Supelco 23462	4.00	0.0100	Sig20488	1875.3	1.6493E-06
Supelco 23462	4.00	0.0100	Sig20489	1987.0	1.6493E-06
Supelco 23462	5.00	0.0100	Sig20490	2324.7	2.0616E-06
CO2 4.0	1.00	0.9999	Sig20850	69482.9	4.1232E-05
CO2 4.0	0.10	0.9999	Sig20851	7390.1	4.1232E-06
CO2 4.0	0.04	0.9999	Sig20852	3477.8	1.6493E-06
CO2 4.0	0.20	0.9999	Sig20886	14671.6	8.2465E-06

Table A.6: GC calibration data for ethane.

Source	Inj. Vol/ mL	mol-frac	Signal File	Area Count·s	C_2H_6 / mol
Supelco 23462	1	0.0101	Sig20282	1858.5	4.206E-07
Supelco 23462	5	0.0101	Sig20415	7921.7	2.103E-06
Supelco 23462	3	0.0101	Sig20416	5592.2	1.262E-06
Supelco 23462	2	0.0101	Sig20422	3821.1	8.411E-07
Supelco 23462	4	0.0101	Sig20424	7877.6	1.682E-06
Supelco 23462	5	0.0101	Sig20439	9911.5	2.103E-06
Supelco 23462	1	0.0101	Sig20442	1992.6	4.206E-07
Supelco 23462	5	0.0101	Sig20444	7841.0	2.103E-06
Supelco 23462	4	0.0101	Sig20488	7244.6	1.682E-06
Supelco 23462	4	0.0101	Sig20489	7460.7	1.682E-06
Supelco 23462	5	0.0101	Sig20490	8917.5	2.103E-06
Supelco 23462	1	0.0101	Sig21088	2065.3	4.206E-07
Supelco 23462	1	0.0101	Sig21089	1934.8	4.206E-07
Supelco 23462	1	0.0101	Sig21090	2103.4	4.206E-07

Table A.7: Integrated peak area for gas syringe samples runs A to N.

Run ID	Sample ID	Carrier Flow	Data File	Method	H_2	CO	CH_4	CO_2	C_2H_6
							counts·s		
A	GSS_1	7.7	Sig21341.D	Air02	304934	1199	37139	13130	
A	GSS_2	7.5	Sig21342.D	Air02	290074	1056	37515	15228	
A	GSS_3	8	Sig21343.D	Air02	297719	860	32516	16067	
A	GSS_4	7.5	Sig21344.D	Air03	309836	855	33811	15564	1667
B	GSS_5	7.4	Sig21345.D	Air02	301683	1030	38702	15075	
B	GSS_6	7.4	Sig21346.D	Air02	296257	1008	38130	15042	
B	GSS_7	7.5	Sig21347.D	Air03	297996	938	38425	15076	3185
C	GSS_8	7.5	Sig21348.D	Air02	293585	817	37917	15210	
C	GSS_9	7.5	Sig21349.D	Air02	299931	699	38350	15657	
C	GSS_10	7.4	Sig21350.D	Air03	297900	682	38198	15216	3658
D	GSS_11	7.5	Sig21351.D	Air02	281583	1437	44790	14875	
D	GSS_12	7.4	Sig21352.D	Air02	277125	1323	43655	14716	
D	GSS_13	7.5	Sig21353.D	Air03	279557	1302	44199	15201	5229
E	GSS_14	7.5	Sig21354.D	Air02	293821	998	41169	15272	
E	GSS_15	7.5	Sig21355.D	Air02	288967	954	40495	15164	
E	GSS_16	7.5	Sig21356.D	Air03	287482	1011	40519	15292	4813
F	GSS_17	7.6	Sig21357.D	Air02	312407	529	33803	15009	
F	GSS_18	7.5	Sig21358.D	Air02	306783	548	36898	15387	
F	GSS_19	7.4	Sig21359.D	Air03	294520	652	38348	15910	3019
G	GSS_20	7.4	Sig21360.D	Air02	299229	615	38603	15587	
G	GSS_21	7.4	Sig21361.D	Air02	294420	582	42057	16012	
G	GSS_22	7.4	Sig21362.D	Air03	295505	630	38721	15452	3985
H	GSS_23	7.4	Sig21363.D	Air02	312496	641	35351	14964	
H	GSS_24	7.4	Sig21364.D	Air02	303634	711	35910	15686	
H	GSS_25	7.4	Sig21366.D	Air03	298589	434	34957	15405	3858
I	GSS_26	7.5	Sig21367.D	Air02	307143	634	37966	14639	
I	GSS_28	7.5	Sig21369.D	Air02	295160	372	39710	14597	
I	GSS_29	7.5	Sig21370.D	Air03	295344	514	36378	14168	3680
J	GSS_30	6.2	Sig21377.D	Air02	365363	365	25504	14171	
J	GSS_31	6.9	Sig21378.D	Air02	324053	864	31835	14232	
J	GSS_32	7	Sig21379.D	Air03	294718		38911	14674	2819
K	GSS_33	7.1	Sig21380.D	Air02	278042	1169	42863	14291	
K	GSS_34	7.1	Sig21381.D	Air02	269588	1095	45921	15240	
K	GSS_35	7.2	Sig21382.D	Air03	279855	1104	47679	15003	5417
L	GSS_36	7.4	Sig21383.D	Air02	323618		31441	15995	
L	GSS_37	7.3	Sig21384.D	Air02	320600	381	35738	13154	
L	GSS_38	7.4	Sig21385.D	Air03	327416		36550	13376	2829
M	GSS_39	7.4	Sig21386.D	Air02	270416	837	43186	13553	
M	GSS_40	7.4	Sig21387.D	Air02	279065	877	43283	14444	
M	GSS_41	7.4	Sig21388.D	Air03	283138	869	47902	15126	4235
N	GSS_42	6.9	Sig21393.D	Air02	257937		40541		
N	GSS_43	7	Sig21394.D	Air02	356274		26581	14400	
N	GSS_44	7.1	Sig21395.D	Air03	321206		30877	16059	2888

Table A.8: Integrated peak area for gas syringe samples runs O to Q.

Run ID	Sample ID	Carrier Flow	Data File	Method	H_2	CO	CH_4 counts·s	CO_2	C_2H_6
O	GSS_45	7.2	Sig21396.D	Air02	304937	655	38673	15199	
O	GSS_46	7.3	Sig21397.D	Air02	295494	651	38203	15446	
O	GSS_47	7.3	Sig21399.D	Air03	295529	594	38572	15027	3945
P	GSS_48	7.3	Sig21400.D	Air02	292793	1233	46571	15619	
P	GSS_49	7.4	Sig21401.D	Air02	282176	1117	44140	14576	
P	GSS_50	7.4	Sig21402.D	Air03	286623	1237	46755	15281	3626
Q	GSS_51	7.4	Sig21403.D	Air02	322054	473	37293	15641	
Q	GSS_52	7.4	Sig21404.D	Air02	318137		37507	15578	
Q	GSS_53	7.4	Sig21406.D	Air03	309303	636	36283	15890	3220

Table A.9: Mean reactor thermocouple (RTC) temperatures, mean reactor pressure.

Run ID	RTC1 T/°C	RTC2 T/°C	RTC3 T/°C	RTC4 T/°C	RTC5 T/°C	RTC6 T/°C	RTC7 T/°C	RTC8 T/°C	Inlet P / psig	Outlet P / psig	Mean Rctr T/°C
A	347.4	546.2	708.7	717.5	691.7	718.1	712.9	687.8	3496.8	3481.4	709.8
B	352.6	517.5	687.8	701.5	677.9	701.4	698.6	674.3	3498.1	3484.9	693.4
C	351.2	520.2	668.9	677.6	656.1	678.0	674.7	653.8	3496.2	3481.6	671.0
D	342.8	525.0	655.2	663.4	642.8	663.8	660.5	639.6	3493.5	3479.9	657.1
E	346.0	503.2	651.7	664.3	644.4	664.2	661.1	640.5	3496.0	3482.5	657.2
F	335.3	482.1	623.9	634.5	616.7	634.6	631.5	614.2	3492.7	3480.7	628.2
G	346.7	523.1	667.8	678.0	655.3	678.3	674.6	652.7	3442.4	3428.8	670.8
H	365.6	496.1	653.5	677.9	656.6	677.7	675.0	654.0	3492.5	3478.8	668.2
I	351.6	528.4	656.9	663.5	642.6	664.1	660.7	641.4	3460.7	3449.5	657.6
J	324.0	533.4	692.9	700.5	674.3	701.4	697.9	674.0	3500.8	3488.0	693.4
K	341.2	525.8	666.2	677.5	653.8	677.7	674.9	652.0	3500.4	3487.2	670.0
L	343.8	511.4	680.2	700.7	675.3	701.2	698.3	674.9	3501.2	3486.2	691.1
M	340.6	562.6	673.6	676.9	651.8	678.0	674.6	651.8	3464.4	3460.1	671.0
N	343.5	512.7	668.6	677.3	654.6	677.8	674.7	654.2	3494.4	3480.5	670.6
O	347.8	525.8	668.0	677.4	654.2	677.7	674.8	653.2	3492.5	3479.6	670.5
P	344.4	550.7	693.1	700.6	674.2	701.3	698.2	672.9	3495.5	3482.3	693.5
Q	352.2	498.0	648.5	663.7	642.6	663.9	661.1	641.4	3509.9	3494.3	656.0

Table A.10: Inlet mass flow rates.

Run ID	Run Start	Run Finish	Run Duration / min	Initial H_2O / kg	Final H_2O / kg	H_2O Rate / $g \cdot min^{-1}$	Initial EtOH / g	Final EtOH / g	EtOH Rate/ $g \cdot min^{-1}$
A	16:35	18:45	130	13.95	12.75	11.43	-24	-122	0.93
B	19:50	21:25	95	11.71	10.34	16.12	-196	-328	1.55
C	21:45	23:25	100	10.1	8.96	11.40	-330	-420	0.90
D	23:40	1:24	104	8.63	7.86	9.17	-450	-580	1.55
E	1:30	3:28	118	7.36	6.12	14.09	-636	-772	1.55
F	14:50	16:33	103	13.92	13.07	11.33	-14	-82	0.91
G	16:43	18:25	102	12.9	11.76	11.40	-86	-178	0.92
H	18:40	20:36	116	11.41	9.34	19.71	-184	-278	0.90
I	20:53	23:04	127	8.99	7.87	9.33	-288	-350	0.52
J	19:15	20:50	95	13.87	13.17	9.33	-8	-54	0.61
K	21:05	22:47	102	12.85	11.83	11.33	-76	-258	2.02
L	0:35	2:18	103	10.93	9.7	13.67	-270	-322	0.58
M	2:35	4:50	135	9.41	8.83	6.44	-362	-444	0.91
N	15:22	17:19	117	7.9	6.69	11.52	-2	-20	0.17
O	17:26	19:18	112	12.82	11.78	11.56	-38	-122	0.93
P	19:30	21:15	105	11.34	10.64	9.33	-172	-288	1.55
Q	21:30	23:15	105	10.45	9.02	13.62	-288	-350	0.59

Table A.11: West test meter data and mean effluent gas flow rate by experiment.

Run ID	Time	Vol / L	t / min	Gas Rate / L min^{-1}	Mean Gas Rate/ L min^{-1}	Run ID	Time	Vol / L	t / min	Gas Rate / L min^{-1}	Mean Gas Rate/ L min^{-1}
A	17:08	9	4.51	2.00		K	21:33	9	2.08	4.33	
A	17:34	9	4.25	2.12		K	21:43	9	2.23	4.04	
A	17:49	9	4.14	2.18		K	21:52	9	2.25	4.00	
A	18:04	9	3.89	2.31		K	22:05	9	2.07	4.35	
A	18:26	9	3.95	2.28		K	22:22	9	2.15	4.19	
A	18:41	9	3.94	2.29	2.19	K	22:34	9	2.13	4.22	
B	20:35	9	2.58	3.48		K	22:43	9	2.21	4.07	4.17
B	20:55	9	2.53	3.55		L	1:08	9	6.64	1.35	
B	21:11	9	2.54	3.54		L	1:20	9	5.87	1.53	
B	21:19	9	2.56	3.51	3.52	L	1:35	9	6.04	1.49	
C	22:25	12	5.83	2.06		L	1:46	9	6.33	1.42	
C	22:45	9	4.36	2.06		L	2:04	9	6.53	1.38	
C	23:06	9	4.53	1.99		L	2:13	6	4.38	1.37	1.42
C	23:21	9	4.59	1.96	2.02	M	3:37	9	4.88	1.85	
D	0:21	9	2.82	3.19		M	3:53	12	6.54	1.83	
D	0:34	9	2.81	3.20		M	4:07	12	5.97	2.01	
D	1:04	9	2.82	3.19		M	4:22	12	6.33	1.90	
D	1:18	9	2.84	3.17	3.19	M	4:32	12	6.34	1.89	
E	2:15	9	2.90	3.11		M	4:44	9	4.70	1.91	1.90
E	2:49	9	2.72	3.31		N	16:28	3	8.98	0.33	
E	3:19	9	2.79	3.23	3.22	N	16:40	3	6.01	0.50	
F	15:24	9	4.39	2.05		N	16:57	4.5	9.90	0.45	
F	15:44	9	4.17	2.16		N	17:15	6	13.74	0.44	0.43
F	15:59	9	4.16	2.17		O	17:55	9	4.25	2.12	
F	16:26	9	4.21	2.14	2.13	O	18:06	9	4.32	2.08	
G	17:16	9	4.46	2.02		O	18:21	12	6.17	1.95	
G	17:35	9	4.15	2.17		O	18:34	9	4.56	1.97	
G	17:47	9	4.35	2.07		O	18:51	12	6.00	2.00	
G	18:02	9	4.44	2.03		O	19:04	9	4.53	1.98	
G	18:18	9	4.48	2.01	2.06	O	19:17	18	8.92	2.02	2.02
H	19:08	9	4.05	2.22		P	20:11	9	2.76	3.26	
H	19:24	9	3.89	2.31		P	20:25	15	4.79	3.13	
H	20:01	9	4.72	1.91		P	20:32	6	1.85	3.25	
H	20:12	9	4.15	2.17		P	20:43	12	3.70	3.25	
H	20:25	9	4.08	2.20	2.16	P	20:54	12	3.78	3.18	
I	21:56	6	5.30	1.13		P	21:10	12	3.81	3.15	3.20
I	22:17	6	4.88	1.23		Q	21:55	3	2.71	1.11	
I	22:47	6	5.14	1.17	1.18	Q	22:11	6	4.73	1.27	
J	19:53	9	6.38	1.41		Q	22:24	6	4.26	1.41	
J	20:06	9	5.83	1.54		Q	22:35	9	6.13	1.47	
J	20:25	9	6.01	1.50		Q	22:51	12	8.22	1.46	
J	20:37	9	6.33	1.42		Q	23:04	9	6.48	1.39	1.35
J	20:49	6	4.56	1.31	1.44						

Table A.12: Liquid effluent collection.

Run ID	Sample ID	Time	Sample Time / min	Mass / g	Q / g·min^{-1}	Q Mean / g·min^{-1}
A	LS200604141725	17:25	16	176	11.00	
A	LS200604141754	17:54	15	172	11.47	11.23
B	LS200604142039	20:39	11	183	16.64	
B	LS200604142101	21:01	10	176	17.60	17.12
C	LS200604142245	22:45	18.5	204	11.03	
C	LS200604142312	23:12	17	178	10.47	10.75
D	LS200604150046	0:46	24	209	8.71	
D	LS200604150112	1:12	20	180	9.00	8.85
E	LS200604150234	2:34	14	186	13.29	
E	LS200604150309	3:09	13	204	15.69	14.49
F	LS200604151546	15:46	18	191	10.61	
F	LS200604151618	16:18	16	174	10.88	10.74
G	LS200604161738	17:38	16	175	10.94	
G	LS200604151809	18:09	16	176	11.00	10.97
H	LS200604151940	19:40	9.5	205	21.58	omitted
H	LS200604152013	20:13	10	178	17.80	
H	LS200604152027	20:27	10	178	17.80	17.80
I	LS200604152122	21:22	18	172	9.56	
I	LS200604152148	21:48	19	162	8.53	9.04
J	LS200604162016	20:16	20	184	9.20	
J	LS200604162038	20:38	12	155	12.92	11.06
K	LS200604162155	21:55	15	172	11.47	
K	LS200604162229	22:29	16	181	11.31	11.39
L	LS200604170126	1:26	14	189	13.50	
L	LS200604170152	1:52	15	201	13.40	13.45
M	LS200604170413	4:13	32	202	6.31	
M	LS200604170446	4:46	33	200	6.06	6.19
N	LS200604171632	16:32	16	186	11.63	
N	LS200604171659	16:59	18	200	11.11	11.37
O	LS200604171827	18:27	16	178	11.13	
O	LS200604171858	18:58	16	184	11.50	11.31
P	LS200604172033	20:33	21	183	8.71	
P	LS200604172105	21:05	21	193	9.19	8.95
Q	LS200604172226	22:26	14	193	13.79	
Q	LS200604172255	22:55	16	212	13.25	13.52

Table A.13: Calculated heater duty by zone.

Run ID	DOE Line	T/K	Zone 1 / Watts	Zone 2 / Watts	Zone 3 / Watts	Zone 4 / Watts	Total / Watts
A	13	982.9	990	468	430	609	2496
B	8	966.6	1220	405	408	579	2613
C	11	944.2	922	399	374	572	2267
D	3	930.3	876	390	368	564	2198
E	7	930.3	1112	352	363	544	2372
F	12	901.4	931	343	335	525	2135
G	10	944.0	950	386	369	573	2278
H	17	941.3	1280	378	393	553	2603
I	1	930.7	802	402	366	570	2139
J	2	966.5	918	462	409	618	2407
K	15	943.2	1019	407	392	560	2378
L	6	964.3	1109	454	419	595	2577
M	16	944.1	640	437	371	580	2028
N	14	943.7	924	418	386	573	2300
O	9	943.6	956	406	390	562	2314
P	4	966.6	897	459	414	602	2372
Q	5	929.1	1012	392	380	546	2331

REFERENCES

1. Perry, R. H.; Green, D. W.; Maloney, J. O., *Perry's chemical engineers' handbook*. Sixth ed.; McGraw-Hill: New York, 1984.
2. API Ethanol Fact Sheet. http://www.api.org/aboutoilgas/otherfuels/upload/Ethanol_Fact_Sheet_07_24_07.pdf (December 4, 2007),
3. Smith, J. M.; Ness, H. C. V.; Abbott, M. M., *Introduction to chemical engineering thermodynamics*. Fifth ed.; McGraw-Hill: New York, 1996.
4. Poling, B. E.; Prausnitz, J. M.; O'Connell, J. P., *The properties of gases and liquids*. Fifth ed.; McGraw-Hill: New York, 2000.
5. Taylor, J. D.; Herdman, C. M.; Wu, B. C.; Wally, K.; Rice, S. F., Hydrogen production in a compact supercritical water reformer. *International Journal of Hydrogen Energy* **2003,** 28, 1171-1178.
6. Lee, S.; Lanterman, H. B.; Wenzel, J. E.; Edwards, N.; Adams, A.; Wootton, J.; Garcia, A., Noncatalytic direct reformation of JP-8 fuel in supercritical water. *Preprints - American Chemical Society, Division of Petroleum Chemistry* **2006,** 51, 487-490.
7. Haryanto, A.; Fernando, S.; Murali, N.; Adhikari, S., Current status of hydrogen production techniques by steam reforming of ethanol: a review. *Energy & Fuels* **2005,** 19, 2098-2106.
8. Fatsikostas, A. N.; Verykios, X. E., Reaction network of steam reforming of ethanol over Ni-based catalysts. *Journal of Catalysis* **2004,** 225, 439-452.
9. Morgenstern, D. A.; Fornango, J. P., Low-temperature reforming of ethanol over copper-plated raney nickel: a new route to sustainable hydrogen for transportation. *Energy & Fuels* **2005,** 19, 1708-1716.
10. Deluga, G. A.; Salge, J. R.; Schmidt, L. D.; Verykios, X. E., Renewable Hydrogen from Ethanol by Autothermal Reforming. *Science* **2004,** 303, (5660), 993-997.
11. Cavallaro, S., Ethanol steam reforming on Rh/Al_2O_3 catalysts. *Energy & Fuels* **2000,** 14, 1195-1199.
12. Klouz, V.; Fierro, V.; Denton, P.; Katz, H.; Lisse, J. P.; Bouvot-Mauduit, S.; Mirodatos, C., Ethanol reforming for hydrogen production in a hybrid electric vehicle: process optimization. *Journal of Power Sources* **2002,** 105, 26-34.
13. Caillot, T.; Gélin, P.; Dailly, J.; Gauthier, G.; Cayron, C.; Laurencin, J., Catalytic steam reforming of methane over $La_{0.8}Sr_{0.2}CrO_3$ based Ru catalysts. *Catalysis Today* **2007,** 128, 264-268.
14. Arita, T.; Nakahara, K.; Nagami, K.; Kajimotoa, O., Hydrogen generation from ethanol in supercritical water without catalyst. *Tetrahedron Letters* **2003,** 44, 1083-1086.
15. Ruettinger, W.; Ilinich, O., Water gas shift reaction. In *Encyclopedia of Chemical processing*, Lee, S., Ed. Taylor & Francis: New York, 2006; Vol. 5, pp 3205-3215.
16. Chase, M. W.; Davies, C. A.; Downey, J. R.; Frurip, D. J.; McDonald, R. A.; Syverud, A. N., JANAF thermochemical tables, third edition. *J. Phys. Chem. Ref. Data* **1985,** 14, (Suppl. 1), 1-1856.
17. Picou, J.; Wenzel, J.; Lanterman, H. B.; Lee, S., Kinetics of non-catalytic water gas shift reaction In a supercritical water medium. In *American Insititute of Chemical Engineers Spring Meeting*, New Orleans, 2008.

18. IAPWS *Release on the pressure along the melting and the sublimation curves of ordinary water substance*; The International Association for the Properties of Water and Steam: Milian, Italy, September, 1993; pp 1-4.
19. IAPWS *Release on the state dielectric constant of ordinary water substance for temperatures from 238 K to 873 K and pressures up to 1000 MPa*; The International Association for the Properties of Water and Steam: September, 1997; pp 1-9.
20. Stryjek, R.; Vera, J. H., PRSV: an improved Peng-Robinson equation of state for pure compounds and mixtures. . *Canadian Journal of Chemical Engineering* **1986,** 64, 323-333.
21. Stryjek, R.; Vera, J. H., PRSV2: a cubic equation of state for accurate vapor-liquid equilibria calculations. . *Canadian Journal of Chemical Engineering* **1986,** 64, 820-826.
22. Abu-Eishah, S., Modification of the predictive capability of the PRSV-2 equation of state for critical volumes of binary mixtures. *Fluid Phase Equilibria* **1999,** 157, 1-16.
23. Hicks, C. P.; Young, C. L., The gas-liquid critical properties of binary mixtures. *Chem. Rev.* **1975,** 79, 119-175.
24. McHugh, M. A.; Krukonis, V. J., *Supercritical fluid extraction: principles and practice*. Butterworths: Boston, 1986; p 507.
25. Kolář, P.; Kojima, K., Prediction of critical points in multicomponent systems using the PSRK group contribution equation of state. *Fluid Phase Equilibria* **1996,** 118, 175-200.
26. Brunner, E.; Thies, M. C.; Schneider, G. M., Fluid mixtures at high pressures: Phase behavior and critical phenomena for binary mixtures of water with aromatic hydrocarbons. *Journal of Supercritical Fluids* **2006,** 39, 160-173.
27. Brunner, E., Fluid mixtures at high pressures: IX. Phase separation and critical phenomena in 23 (n-alkane + water) mixtures. *J. Chem. Thermodyn.* **1990,** 22, (4), 335-353.
28. Shmonov, V. M.; Sadus, R. J.; Franck, E. U., High-pressure phase equilibria and supercritical pVT data of the binary water + methane mixture to 723 K and 200 MPa. *J. Phys. Chem.* **1993,** 97, 9054-9059.
29. Sadus, R. J., *High pressure phase behaviour of multicomponent fluid mixtures*. Elsevier: Amsterdam, 1992; p 392.
30. Heidemann, R. A.; Khalil, A. M., The calculation of critical points. *AIChE Journal* **1980,** 26, 769-779.
31. Boukis, N.; Diem, V.; Habicht, W.; Dinjus, E., Methanol reforming in supercritical water. *Ind. Eng. Chem. Res.* **2003,** 42, 728-735.
32. Factor, M. J.; Lanterman, H. B.; Wenzel, J. E.; Lee, S., Use of haynes alloy 230 for supercritical Water reactors. In *American Insititute of Chemical Engineers Annual Meeting*
Salt Lake City Utah, 2007.
33. Kritzer, P.; Boukis, N.; Dinjus, E., The corrosion of nickel-base alloy 625 in sub- and supercritical aqueous solutions of oxygen: a long time study. *Journal of Materials Science Letters* **1999,** 18, 1845-1847.
34. *Technical Bulletin, SMC-063*; Special Metals Corporation: New Hartford, NY, January 2006, 2006.
35. Lee, S., *Methane and its derivatives*. Marcel Dekker: New York, 1997; p 415.

36. Box, G. E. P.; Hunter, W. G.; Hunter, J. S., *Statistics for experimenters : an introduction to design, data analysis, and model building* Wiley: New York, 1978; p 653.
37. Detector Systems. In *HP 5980A Gas Chromatograph Reference Manual*, 8th ed.; Hewlett-Packard Company: Avondale, Pennsylvania, 1986; Vol. 1.
38. Lee, S.; Lanterman, H.; Wenzel, J.; Picou, J.; Factor, M.; Leavitt, L., Global kinetics of supercritical water reformation of JP-8 fuels. *Preprints-American Chemical Society, Division of Petroleum Chemistry* **2006,** 51, 521-523.

VITA

Jonathan Evar Wenzel was born on November 10, 1975 in Belvidere, Illinois to Kurt and Donna Wenzel. During Jonathan's childhood, his family lived in multiple locations throughout the Midwest including Rockford and Mt. Morris in Illinois, Hutchinson, Kansas, and Chillicothe, Missouri. Jonathan graduated in 1994 from Chillicothe High School. He then went to college at the University of Missouri—Columbia where he received his Bachelor's of Science in Chemical Engineering in 1999. Jonathan currently works as an Assistant Research Engineer for Dr. Sunggyu Lee in the Department of Chemical and Biological Engineering at the Missouri University of Science and Technology in Rolla, Missouri.